Initiation and Evolution of an Intense Upper-Level Front

FREDERICK SANDERS

Marblehead, Massachusetts

LANCE F. BOSART AND CHUNG-CHIENG LAI*

State University of New York at Albany, Albany, New York

(Manuscript received 24 July 1990, in final form 30 November 1990)

ABSTRACT

Within confluent northwesterly flow of an intensifying baroclinic wave over North America in late October 1963, an intense frontal zone developed in 12 h near the inflection point in the middle and upper troposphere. By 24 h after its initial appearance, the zone extended roughly from 400 to 700 mb and from the inflection point to just beyond the downstream trough. Horizontal gradients of potential temperature reached 15–20 K $(100\ \text{km})^{-1}$. Air within the frontal zone was extremely dry.

As the accompanying trough approached the east coast of the United States, surface frontogenesis occurred offshore, remaining distinct from the upper-level front. A region of subsidence, elongated in the direction of the upper-level flow, displayed maximum descent on the warm edge of the frontal zone and played a frontogenetical role through tilting of the isentropic surfaces.

Analysis of isentropic potential vorticity showed significant increase of this quantity near the cold base and a probable decrease near the top as the front developed. Turbulent heat flux, associated with reduced Richardson numbers within the frontal zone, was likely responsible for this nonconservation of potential vorticity and for the propagation of the zone to lower colder values of potential temperature.

Vertical wind shear through the frontal layer was supergeostrophic in the upper ridge and subgeostrophic in the trough. An inertial oscillation at the top of the layer began as air in the ridge flowed toward lower geopotential, forming a jet streak and then flowing toward higher geopotential near the inflection point, a region of intense individual frontogenesis.

1. Introduction

In a review paper on upper-level fronts, Keyser and Shapiro (1986) stated the need for documentation of frontal evolution through the life history of the baroclinic wave in which the front is embedded, in order to provide a synthesis for the many fragmentary views provided by earlier studies. They further called for (i) determination of the relative importance of two-dimensional and three-dimensional processes in frontogenesis, (ii) assessment of the importance of dynamical mechanisms not accounted for by the geostrophic momentum approximation, (iii) study of the interaction between upper-level frontogenesis and baroclinic wave amplification and (iv) study of associated developments, including cyclogenesis, in the lower troposphere.

An opportunity to address these needs arose in October 1963, when a clear and simple case occurred within the North American rawinsonde network. Our goals are to provide the documentation called for and to examine the other three issues mentioned. Our study of the evolution of the front in the temperature field and the associated ageostrophic vertical wind shear showed, in addition, characteristics of the upper frontogenesis and frontal evolution not generally appreciated, although perhaps not generally applicable.

A minimal outline of the situation on the synoptic scale is provided in Fig. 1. The selected contour followed approximately the belt of maximum wind at 500 mb. In the mainly zonal flow pattern on 27 October, a small disturbance grew rapidly as a baroclinic wave. The growth was first apparent in ridge amplification near the West Coast beginning at 0000 UTC on the 27th (2700). The downstream trough began to plunge southward by 2800. Its deepening was nearly completed 24 h later, at which point the next ridge downstream erupted poleward along the East Coast. Hurricane Ginny, which had developed earlier as a tropical depression in the southeastern Bahamas, turned slowly toward the northeast just prior to baro-

* Present affiliation: Institute for Naval Oceanography, Stennis Space Center, Mississippi.

Corresponding author address: Dr. Frederick Sanders, 9 Flint Street, Marblehead, MA 01945.

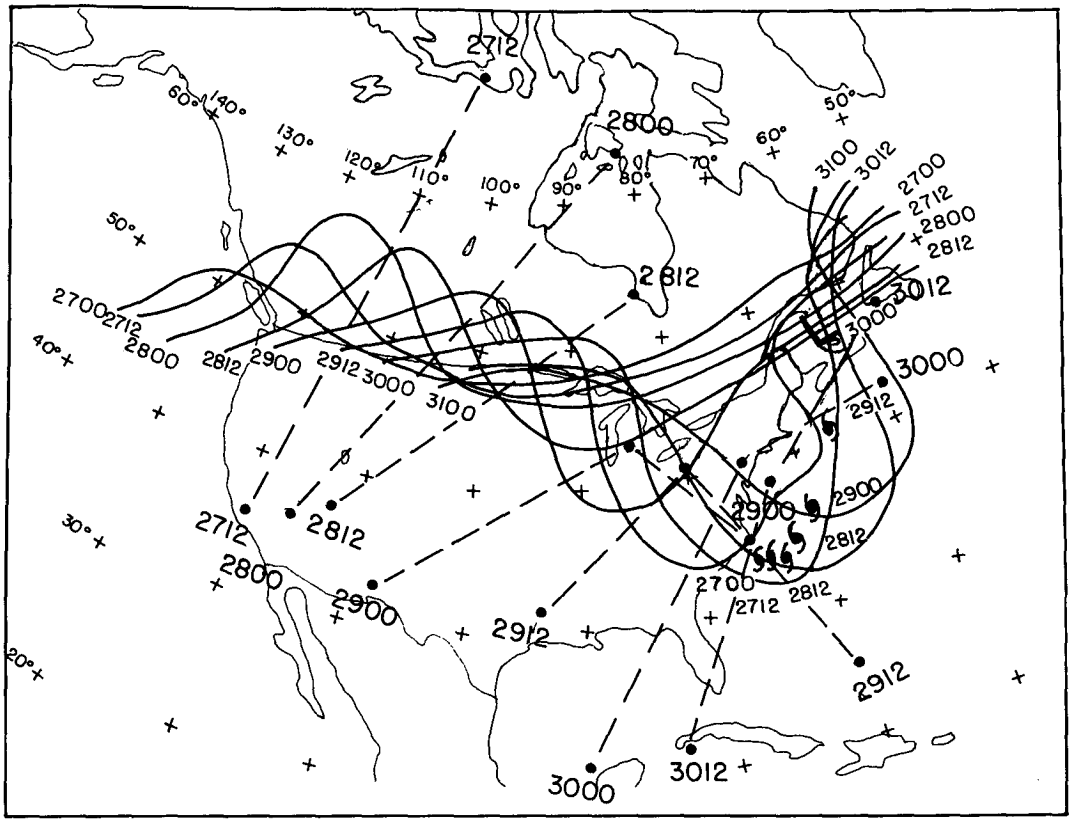

FIG. 1. Positions of the 552-dam height contour at 500 mb for the October 1963 dates and UTC times shown by the four digits. Positions of Hurricane Ginny are shown each 12 h from 2700 through 3000, after which it lost its identity. The dashed lines show the positions of the vertical cross sections of Fig. 3, with date and time.

clinic trough development about 2000 km to the northwest and accelerated as an extratropical cyclone.

2. The temperature field

Broad-scale analyses based on gridpoint data from the National Meteorological Center did not show strong growth of temperature gradient. Over distances of 555 km the maximum values of contrast in the area of the trough varied between 10° and 15° C at 500, 700, and 850 mb. At 300 mb this contrast did not exceed 10°C.

To take advantage of the detailed vertical profiles of temperature provided by the rawinsonde observations, we prepared sets of isentropic charts for 4-K intervals of virtual potential temperature between 279 and 327 K from 2712 through 3012. Analyses of station pressure and surface potential temperature served as a lower boundary condition. Isobaric analysis was quite straightforward and simple. The places of greatest uncertainty over the continent were near the intersections of the isentropic surfaces and the ground at 0000 UTC, when adiabatic lapse rates occurred.

Since an isobar on an isentropic surface is an isotherm on a constant-pressure surface, the temperature fields are thus implicit. The implied patterns on constant-pressure surfaces are detailed, because the horizontal gradient at a point is given by the product of vertical gradient of temperature, which is known in detail at the sounding locations (and usually shows reasonable continuity on a given isentropic surface from station to station), and the slope of the isentropic surface obtained from the large-scale analysis.

The examples in Fig. 2 illustrate the evolution of the temperature field. Between 2800 and 2812, the gradient at 300 mb strengthened and moved north as the ridge continued to build at this level. At 500 mb there was little change, while gradients weakened slightly at 700 mb. The beginning of trough amplification at 2812 was not preceded by, and did not immediately result in, upper-level frontogenesis.

Between 2812 and 2900 the maximum gradient at 300 mb weakened. At 500 mb the opposite happened. A coherent band of very strong temperature gradient appeared in the northwesterly flow, with strong cyclonic shear on the left flank of the associated 55 m s^{-1} jet. Cursory inspection of the 500-mb patterns at these two times indicates that development of the gradient was associated with strong adiabatic warming in the northwesterly flow, since the temperature on the warm side of the zone of contrast at the later time was higher than the temperature anywhere upstream earlier. Gradients strengthened only slightly at 700 mb.

This initial development evidently occurred in an environment of confluence and slight warm advection, to judge from conditions in south-central Canada at 500 mb at 2812 (Fig. 2b) just upwind from the location where the strong contrast appeared at 2900. At the same time, Fig. 2b shows cold advection at and immediately upstream from the 500-mb trough. Thus the mechanism considered by Keyser and Pecnick (1985) in a two-dimensional modeling study, which relies on cold advection and confluence, may have contributed downstream from the region of most intense individual frontogenesis.

By 2912 the temperature gradient at 300 mb had become further disorganized. A small but intense cold center had developed east of the geopotential trough. At 500 mb the zone of intense gradient had become stronger and lengthened from near the inflection point in the northwesterly flow into the trough, while at 700 mb the gradient strengthened.

A more comprehensive view of the evolution of the temperature field is presented in Table 1. For reference it should be noted that a 500-km distance for a contrast of 12 K represented approximately the maximum gradient shown in the broad-scale analyses discussed earlier. The distance should be much smaller for the structure to be regarded as distinctly frontal.

(i) 300 mb: There was never a marked frontal structure, aside from the edge of the small cold core noted above that appeared after the development of the frontal zone at lower levels.

(ii) 400 mb: Substantial strengthening of contrast had occurred by 2812, with further intensification of the frontal zone to follow in the next 24 h. The particularly strong gradient at 3000 was a reflection of the 300-mb cold core.

(iii) 500 mb: The dramatic compression of the temperature contrast into a prominent frontal zone at 2900, as seen in Fig. 2c, was followed by further intensification in the next 12 h.

TABLE 1. Minimum horizontal distance for 12-K contrast in virtual potential temperature, from upper ridge to downstream trough. The number in parentheses is potential temperature, at center of 12-K range.

	Time						
p (mb)	2712	2800	2812	2900	2912	3000	3012
300	510	465	377	400	266	89	100
	(313)	(313)	(313)	(317)	(325)	(321)	(321)
400	499	299	211	177	155	94	200
	(305)	(313)	(305)	(309)	(309)	(309)	(313)
500	443	310	321	100	66	72	122
	(301)	(301)	(305)	(305)	(307)	(305)	(309)
700	476	388	488	400	144	78	355
	(297)	(301)	(297)	(297)	(297)	(301)	(305)
850	753	543	710	544	211	588	755
	(293)	(301)	(293)	(297)	(293)	(297)	(297)
Surface	599	311	444	455	344	511	133
	(285)	(301)	(289)	(297)	(289)	(293)	(285)

(iv) 700 mb: The development of an intense frontal zone between 2900 and 3000 lagged the similar development at 500 mb by 12 h, and nearly matched its intensity.

(v) 850 mb: There was little evidence of a frontal zone, except briefly and modestly at 2912.

(vi) Surface: In or west of the upper trough, no gradients were intense enough to be regarded as frontal zones until 3012. The situation at this time was not frontal, however, since the contrast was between nocturnally cooled air over land along the Gulf Coast and air heated offshore. The airflow was northeasterly with anticyclonic curvature, contrary to what would be expected at a front.

For further illustration of the frontal development, at each time from 2712 to 3012 a vertical cross section was prepared from the isentropic analyses along a line normal to the isotherms where the tropospheric gradient was strongest. The section lines are shown in Fig. 1. The first three of these extended from the warm ridge in the southwestern United States across the northwesterly flow to the core of the cold air in Canada. The remaining lines bent on reaching the center of the cold trough and ran southeastward through a developing frontal zone east of the trough. This front was associated with precipitation, whereas the zone in the northwesterly flow was characterized by clear skies. The patterns of virtual potential temperature, and of relative humidity and observed wind component normal to the section (from sounding stations near the line), are shown in Fig. 3.

The frontal temperature gradient first appeared between 400 mb and 550 mb at 2900 (Fig. 3d). It did not form initially at a preexisting tropopause, as defined by the World Meteorological Organization (WMO), but a lower (and potentially colder) tropopause was shown at its upper end at 2900. Strong cyclonic wind shear and stability were seen below and poleward of the jet core for 36 h before this time however, indicating an extension below the WMO tropopause of isentropic potential vorticity (IPV) large enough to be regarded as stratospheric (Hoskins et al. 1985). The similarly large values of IPV in the upper portion of the developing frontal zone suggest a stratospheric origin for this air, as noted by Reed and Sanders (1953). An examination of prior Canadian soundings upwind from this region, however, failed to disclose a tropopause or strong stratification on the 299-K and 303-K isentropic surfaces seen just above the polar tropopause in Fig. 3d. Examples are the soundings shown in Figs. 15a and c and the 2812 sounding at 72867 (not shown), which displayed a distinct tropopause at 307 K.

Thus, a stratospheric origin might be questioned, at least for part of the air in the frontal zone. However appealing a metaphor "tropopause folding" might be, it does not seem to describe adequately the developmental aspects of this case. A quantitative analysis of IPV will be shown presently.

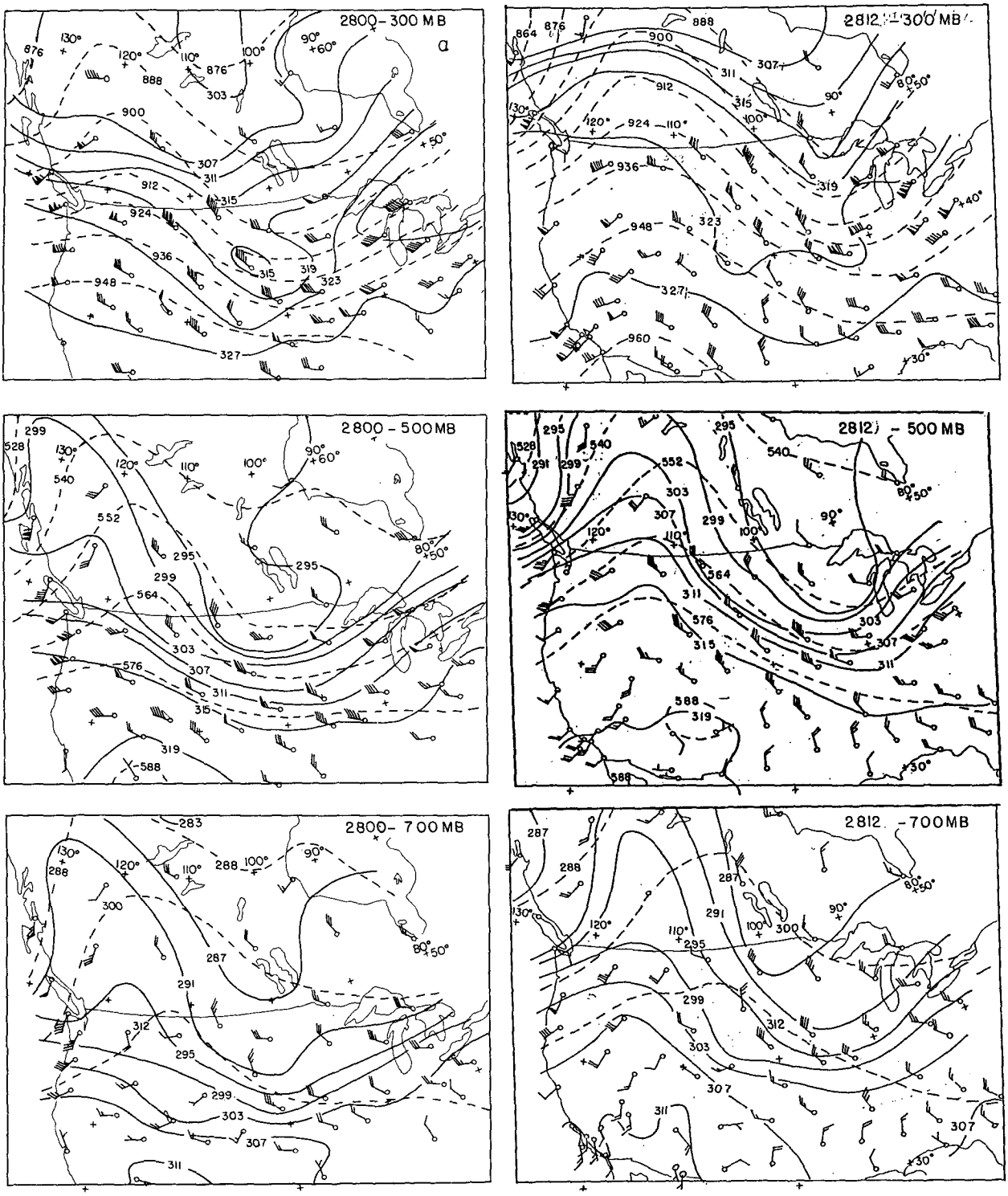

FIG. 2. Analyses at specified pressure levels, (a) 2800, (b) 2812, (c) 2900, and (d) 2912. Solid lines are isotherms of virtual potential temperature at intervals of 4 K. Dashed lines are height contours at intervals of 12 dam. Observed winds are plotted in the conventional manner, with a full barb representing a speed of 5 m s^{-1}. The position of Hurricane Ginny is indicated at 2900 and 2912.

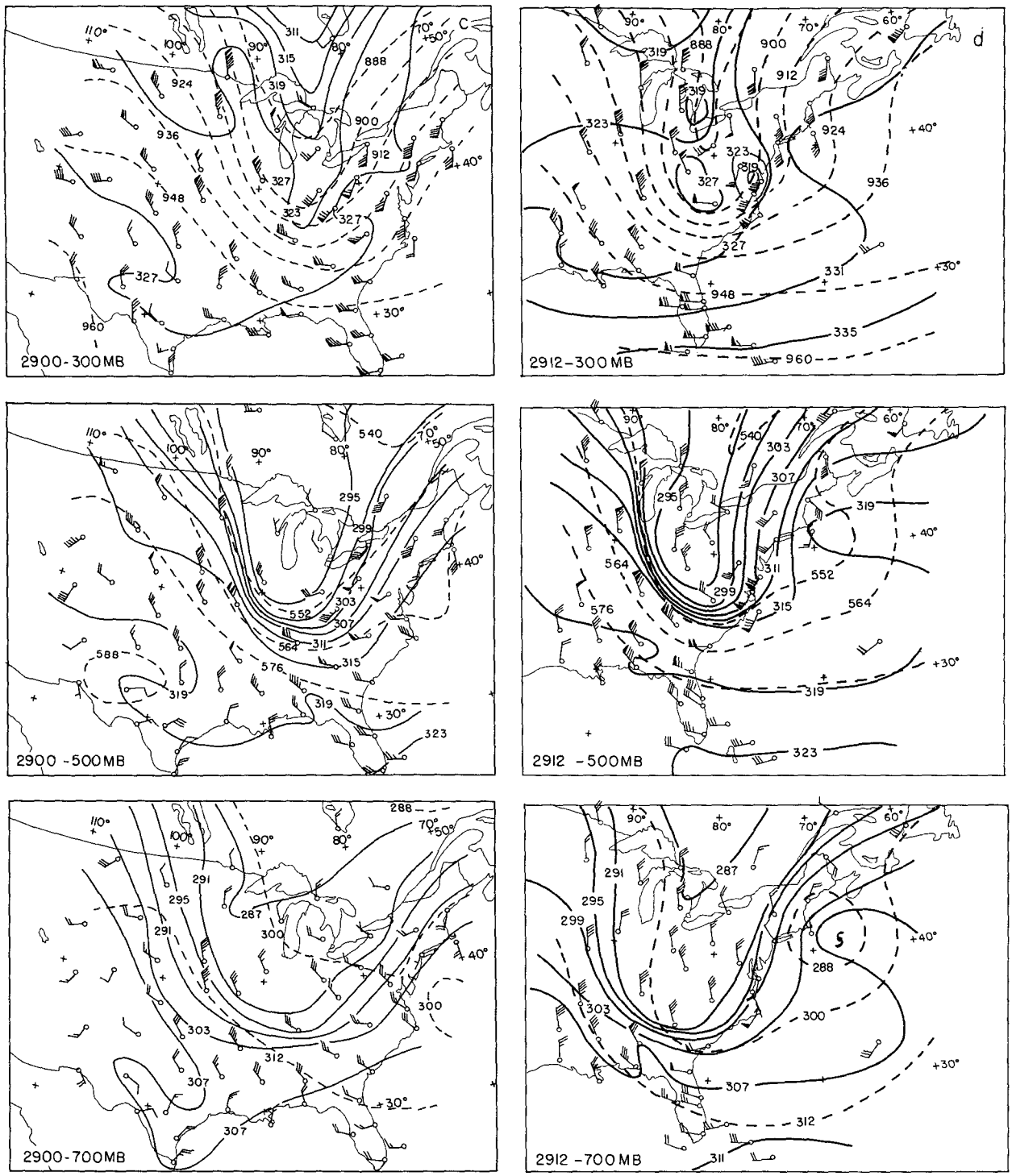

FIG. 2. (*Continued*)

Twenty-four hours later (Fig. 3f) the frontal zone had developed downward to include the 700-mb level, but had begun to weaken at 400 mb. The intense cold dome above 400 mb evolved between 2912 and 3012 (Figs. 3e–g).

The down propagation of the zone was accompanied by migration to lower potential temperatures, but the structure was continuous from the upper troposphere down to the 800-mb level. The later development of the intense gradient near 300 mb occurred at higher

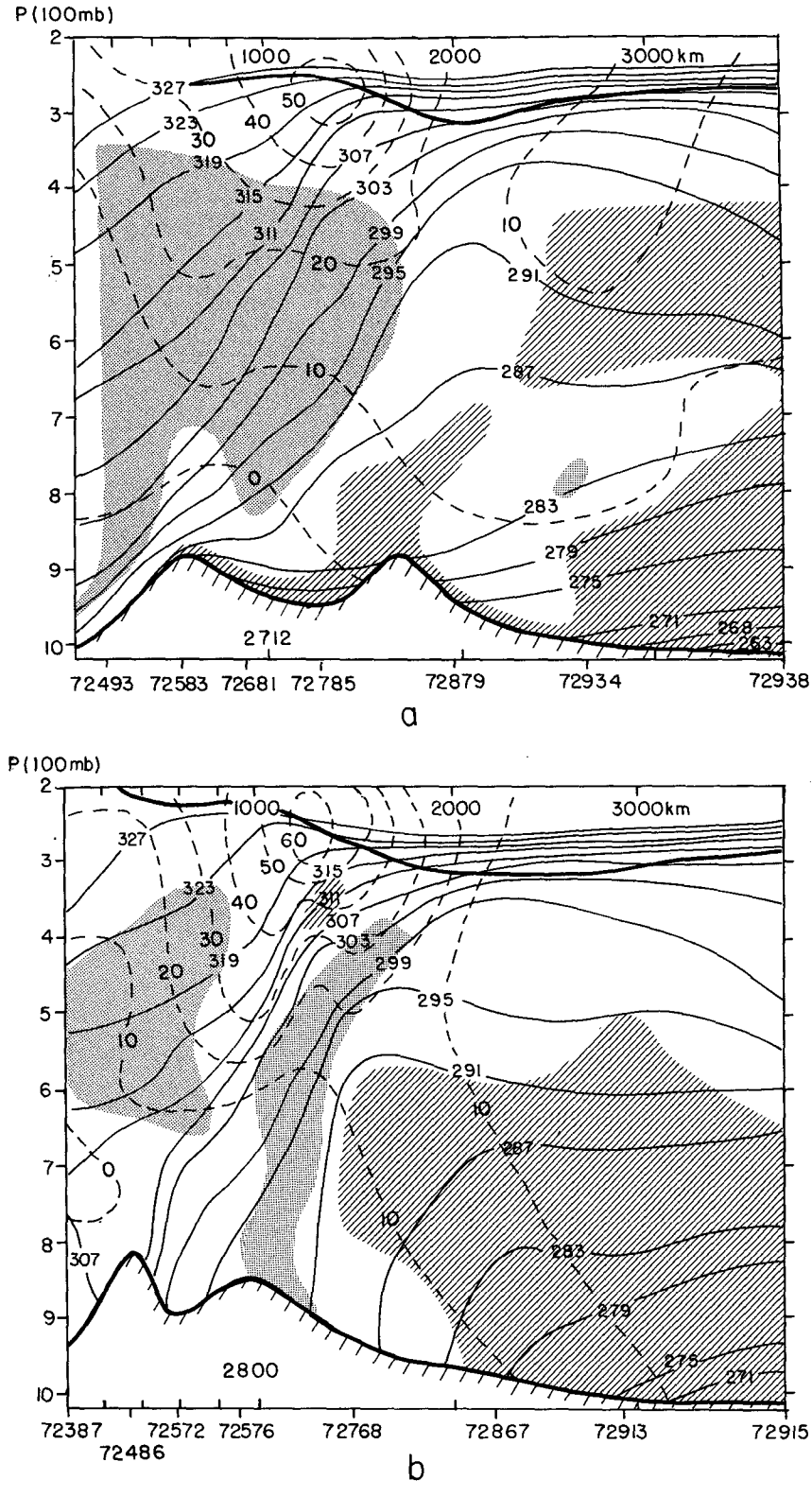

FIG. 3. Vertical cross sections along the dashed lines in Fig. 1, from 2712 (a) through 3012 (g). Solid lines are potential isotherms at intervals of 4 K. Dashed lines are isotachs of the observed wind component normal to the section plane, at intervals of 10 m s^{-1}. In parts (d)–(g) the section line changes direction at the cold trough. To the left, positive wind components are out of the section plane; to the right they are into it. Stippling indicates relative humidity $\leq$ 20%, hatching $\geq$ 60%. Heavy solid lines represent the surface at the bottom and the WMO tropopause (where present) at the top.

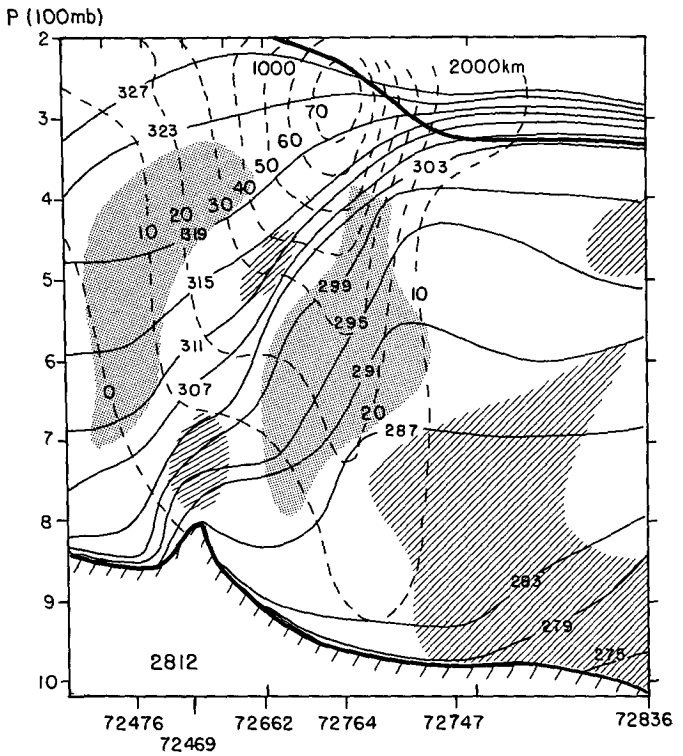

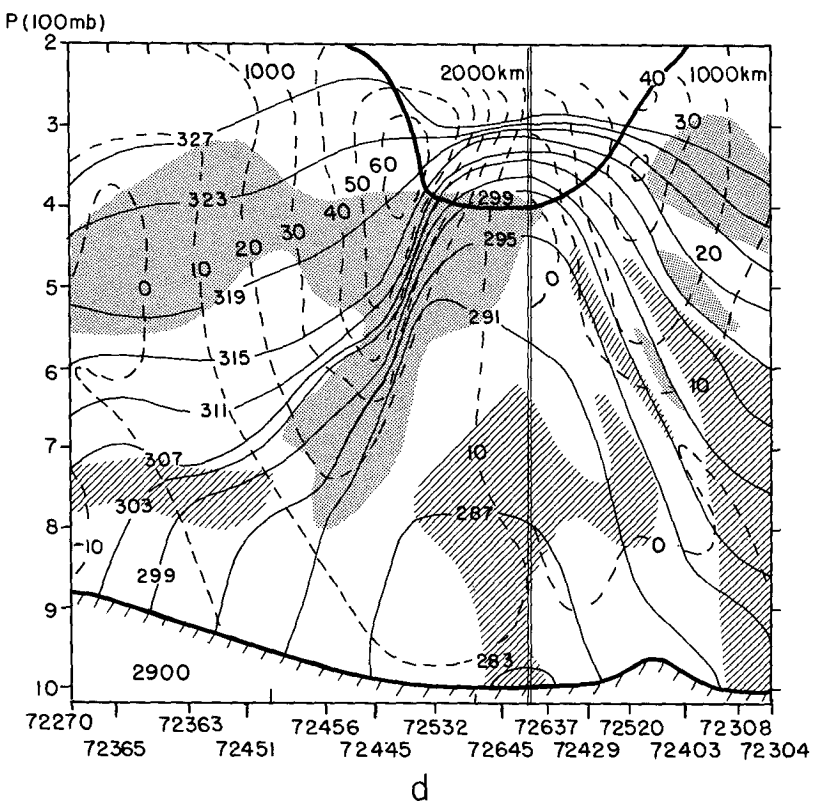

FIG. 3. (*Continued*)

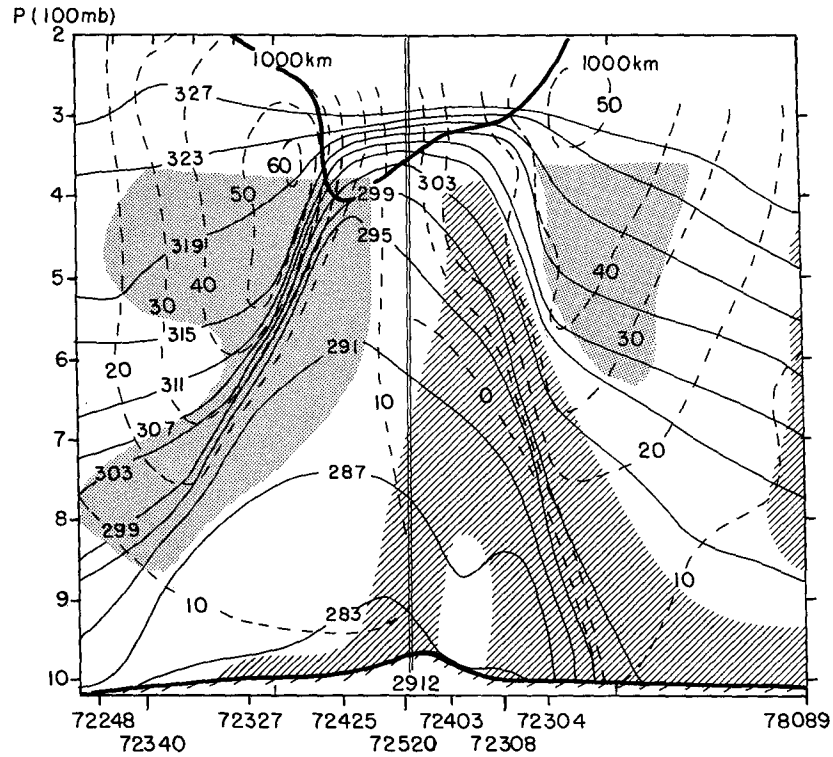

e

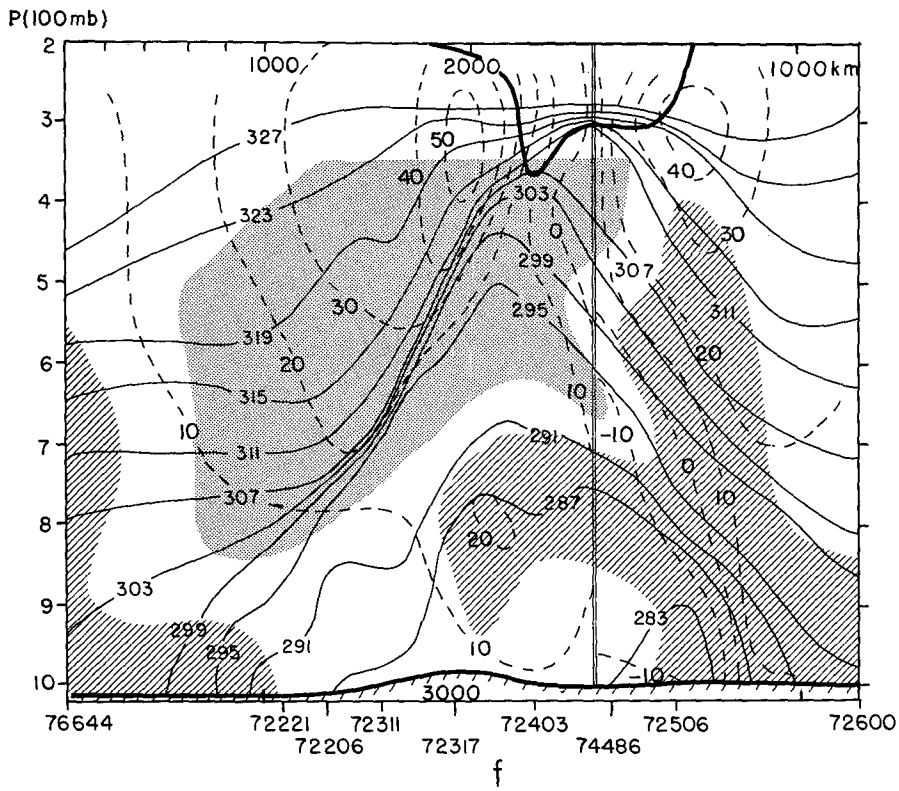

f

FIG. 3. (*Continued*)

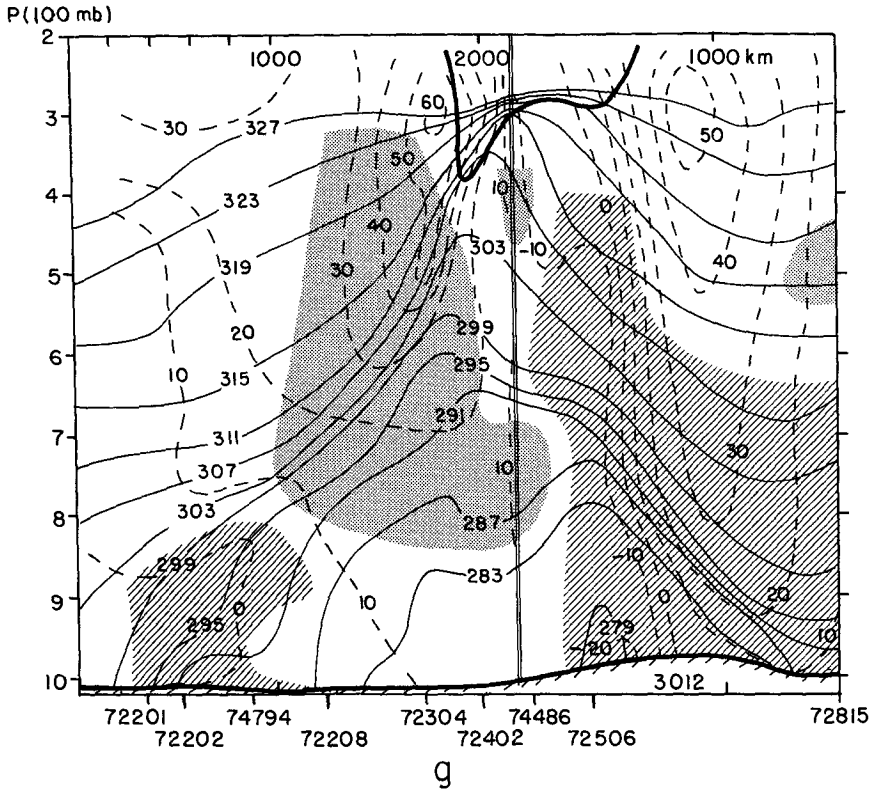

FIG. 3. (*Continued*)

potential temperatures and appeared to be separate from the main feature.

Note in Figs. 3a–c and in Figs. 2a,b the relatively strong horizontal gradient in the middle troposphere between the 303-K and 311-K potential isotherms, prior to the main event. A bit of this structure could still be seen in Fig. 3d. The relative humidity in this feature was higher on the warm side of this contrast, suggesting it was a consequence of confluence in the flow just east of the ridge. The main frontal zone, however, was extremely dry. Humidities were higher in the cold dome throughout the episode.

The frontal structure formed in the northwesterly flow was transported into the base of the trough and beyond. Weakening was underway at all levels by 3012, as seen in Table 1, so in this case the further strengthening sometimes seen (e.g., Reed 1955; Bosart 1970) in confluent flow ahead of the trough did not occur. The flow was difluent (Figs. 2c,d), as well as can be judged over the data-sparse western Atlantic. The few soundings at offshore locations, however, failed to show the intense frontal structure seen earlier over the continent.

Note in Fig. 3 that the northwesterly jet core did not become systematically stronger as the upper front developed. Maximum strength was reached at 2812, prior to the appearance of the intense frontal temperature gradients. These gradients were accompanied by increasingly concentrated vertical shear, as required by the thermal-wind relationship, but the strength of the baroclinic zone in a broad sense did not increase.

East of the cold trough another baroclinic zone associated with a surface front grew but never achieved the intensity of the upper-level front. Keyser and Shapiro (1986) note the difficulty in determining the degree to which these two types of front merge. In this case a sounding is available where this merger might be expected to have occurred. It was used in the cross section for 2912 (Fig. 3e). East of the trough very dry air overlay nominally saturated air, with distinct baroclinic zones in each layer, indicating lack of merger.

The key sounding, for 72304, is shown in Fig. 4. Note the moist stable layer between 900 and 750 mb, and the dry isothermal layer from 600 to 550 mb, both accompanied by strong vertical wind shear. The lower frontal zone extended downward to the surface, while the higher, with winds from 30–45 m s^{-1}, was a part of the upper-level front that had traveled around the trough. Examples from other cases were presented by Sanders (1954). Of course, if one stands back far enough one could say that merger had occurred, but the structures were in fact separate.

This is not to say that there were no low-level consequences of the upper-level development. Conditions

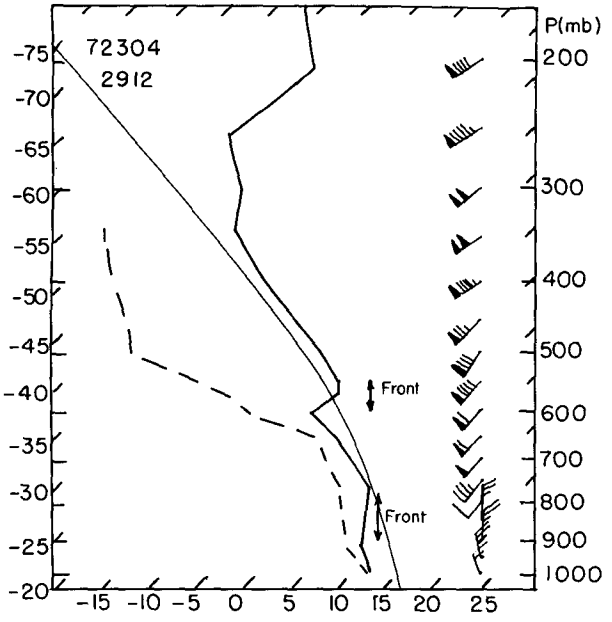

FIG. 4. Skew T–log$p$ diagram of the 2912 sounding from Hatteras, showing the lower and upper fronts. The solid and dashed lines represent temperature and dewpoint respectively. The thin solid line is a saturation adiabat. The winds are plotted as in Fig. 2.

at the surface at 2912 offshore from the mid-Atlantic States are shown in Fig. 5, while conditions at upper levels appear in Fig. 2d. Hurricane Ginny was associated with its own upper-level perturbation and was moving rapidly north-northeastward, leaving a surface trough behind along the Gulf Stream. As the 500-mb trough containing the upper-level front approached the coast near Hatteras, a surface cold front and new low center developed in this surface trough. Note that it had its own separate area of precipitation and deep convection. By 3012 (not shown) a weakening remnant of Ginny was crossing the northern coast of the Gulf of St. Lawrence, while the new cyclone had deepened about 20 mb, moving to near 43°N, 66°W as the upper trough overtook it (c.f., Fig. 1). Evidence of the associated moist frontal zone can be seen aloft in the cross-sections, Figs. 3e–g.

This cyclogenesis fits the typical pattern for the region presented by Sanders (1986). In that study, a correlation between surface deepening rate and 500-mb cyclonic vorticity advection was shown. In this case, the peak cyclonic advection was probably more intense than it would have been without the presence of the upper front, but we can only speculate about the effect on the deepening of the surface cyclone, because other factors are involved as well.

3. Isentropic trajectories and vertical motions

Two isentropic surfaces, for 311 and 295 K, were selected to represent conditions in the mature upper frontal zone, near its warm and cold boundaries. Wind velocities, originally at 50-mb intervals, were interpolated to the pressures of the set of analyzed isentropic surfaces. A number of trajectories along each of these selected surfaces were estimated within and near the large area of descending northwesterly flow, during 12-h periods beginning at 2800, 2812, and 2900.

Most of the trajectories were traced backward from endpoints at rawinsonde stations, while a few were traced forward from stations. Thus, conditions were known at one end or the other of the trajectory without the uncertainty associated with analysis. For backward trajectories a 6-h displacement at the observed velocity was projected upstream. This midpoint was transferred to the map 12 h earlier, on which a point was sought such that the velocity, interpolated among the observations, would produce a straight 6-h forward displacement from that point to the previously determined midpoint. For forward trajectories, an analogous process was used.

For most of the trajectories, the wind observations were sufficiently dense that interpolation could be done with little reference to the geostrophic wind field. In Canada, however, some reliance on the geostrophic field was unavoidable.

The technique used, although not based on an attempt to reconcile acceleration with ageostrophic flow, as described by Petersen and Uccellini (1979), is probably as accurate as can be done with information only at 12-h intervals. The primary importance of this limitation was noted by Uccellini et al. (1984). The errors of approximation will at least tend to counteract each other in the two segments. In this study, moreover, many of the trajectories showing the largest subsidence occurred in nearly straight northwesterly flow and are free of the uncertainty associated with large velocity differences between the two trajectory segments. The vertical displacement, obtained by differencing the isentropic pressures at the ends of the trajectory, was attributed to the midpoint. The results are shown in Fig. 6 for the interval from 2812 to 2900.

As a check, the quasi-geostrophic (QG) omega equation was solved three-dimensionally at 850, 700, 500 and 300 mb on a 1° lat–long horizontal grid covering most of North America and adjacent oceanic sectors. The calculation was based on the broad-scale analyses that did not reveal the intense front. Omega was set to zero at all boundaries, and static stability was taken as a horizontal average over the domain at each pressure level. Solutions were obtained at 12-h intervals and were averaged at 500 mb for comparison with the isentropic results. They appear also in Fig. 6.

From the trajectories, there was a broad area of descent west of the Great Lakes, elongated roughly along the flow (as in the channel-model calculation of Keyser et al. 1989) and of comparable strength at both levels. The trajectories selected for illustration include those terminating at stations 72451, 72456, 72445 and

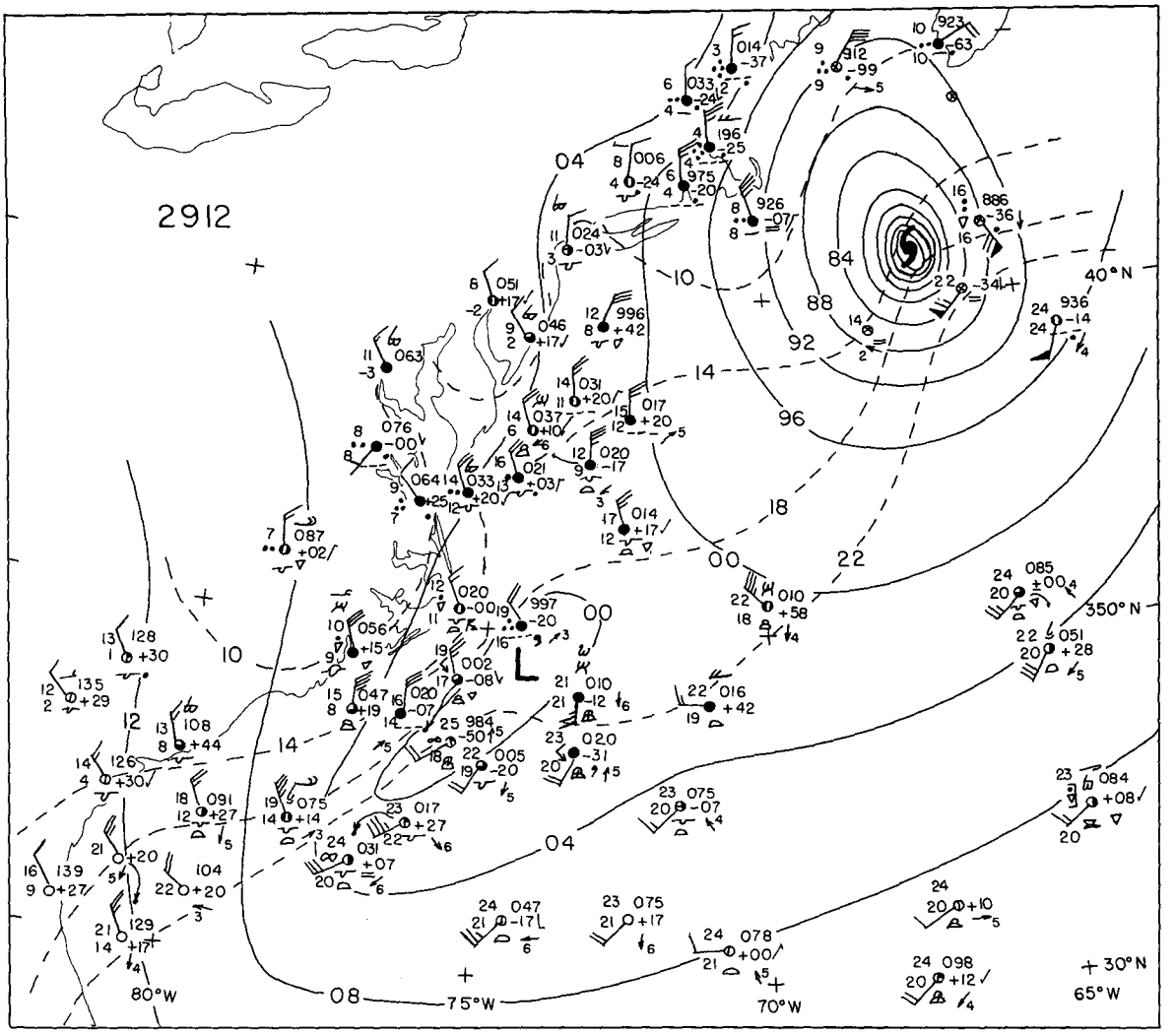

FIG. 5. Surface map for 2912. Solid lines are isobars at 4-mb intervals labeled with the tens and units of millibars. Dashed lines are isotherms at intervals of 4°C, chosen to correspond approximately to the potential isotherms in Figs. 2 and 3.

72532, near the line of the cross section (Fig. 3d) showing the initial appearance of the front. Those arriving at 72456 and 72445 showed the greatest descent, explaining the downward-bowed shape of the isentropic surfaces in this area in Fig. 3d, and indicating the importance of the gradient of subsidence in creating horizontal temperature gradient northeast of these stations.

At both levels there was an indication of a double center (very weak on the 295-K surface in Fig. 6), one in the United States and the other in Canada. The pattern of QG vertical motion is seen in Fig. 6 to be roughly consistent with the southern center of adiabatic descent. The coarse temperature analysis showed the strong gradient in the northwesterly flow much weaker and slightly farther east than it actually was. Thus it is not surprising that the quasi-geostrophic center was somewhat weaker and slightly farther east than the center found by the adiabatic method applied to detailed analyses.

On the other hand, there was no indication in the QG pattern, at either 500 or 300 mb (not shown), of the northern center of subsidence in Canada, particularly pronounced on the 311-K surface. We believe this is a manifestation of highly ageostrophic upper-tropospheric flow in the ridge, of great importance to the frontogenesis and to be discussed later.

Between the 12-h intervals preceding and following the one illustrated, the maximum subsidence from the trajectories grew only modestly at 311 K, and not at all at 295 K, despite considerable growth in the amplitude of the wave. This behavior also characterized the idealized calculation by Keyser et al. (1989). The southern center moved east-southeastward at 13 m s^{-1} from the preceding interval and then south-southeast-

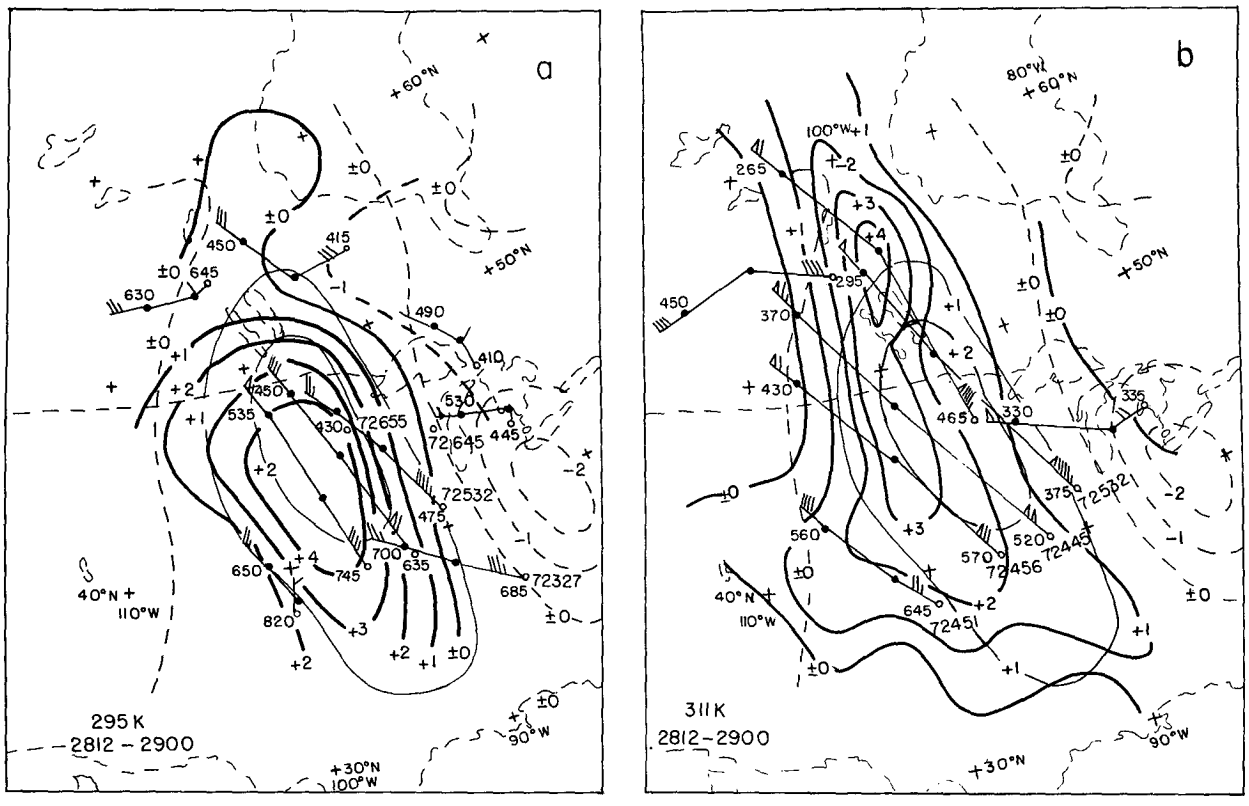

FIG. 6. Estimates of vertical motion (μb s^{-1}) derived from 12-h changes in pressure along trajectories on the 295-K (a) and 311-K (b) isentropic surfaces from 2812 to 2900, and from quasi-geostrophic diagnosis, averaged to represent conditions at 2818. The heavy solid lines represent values from the isentropic trajectories. The thin lines refer to the diagnosis, solid for positive and dashed for zero or negative values. Initial and final winds and pressures, and midpoints, are shown for selected trajectories.

ward at 23 m s^{-1} in the interval following the one illustrated. The northern center moved similarly, tending to lose its identity in the last interval. The essentially meridional elongation of the area in Fig. 6 was seen in all three intervals. The center of QG subsidence tracked similarly, but grew substantially as the geopotential trough increased in intensity. This growth of QG subsidence is probably unrealistically large, since the wind in the trough was markedly subgeostrophic and the geostrophic forcing was thus an overestimate.

The sudden appearance of extremely strong temperature gradient at 500 mb at 2900 can be attributed in part to the eastward motion of the subsidence region relative to the zone of maximum temperature gradient as shown in Table 1. In the interval from 2800 to 2812, the maximum descent lay close to the center of the zone, so that differential subsidence was not effective in enhancing it. By close comparison of Figs. 2b,c with Fig. 6, it can be seen that the maximum subsidence between 2812 and 2900 lay near the warm edge of the zone and was acting frontogenetically. This relative orientation remained during the next 12-h interval. The enhanced vertical gradient of potential temperature around the 295-K surface (c.f., Figs. 3c,d) also strengthened the frontogenetical effect of the differential subsidence.

The subsidence, as it moved eastward, was responsible for the 9 m s^{-1} eastward propagation of the upper front from 2900 to 3000. This could not be accomplished by horizontal advection, because within the frontal zone the wind component normal to the isotherms was insufficient.

From the broad-scale analyses of height and temperature (not shown), and the QG vertical motions, calculations were made of the scalar rate of frontogenesis, following the parcel. It was found that the rates due to horizontal confluence and tilting were of comparable magnitude. The results were not enlightening, however, because the coarse analysis did not detect the strength of the frontal zone. No instantaneous detailed vertical motions were available for calculations of frontogenetical rates from the detailed temperature analyses.

4. Isentropic potential vorticity

In view of the renewed interest in IPV stimulated by Hoskins et al. (1985), and since Reed and Sanders (1953) and subsequently many others have noted anomalously high values in upper-level frontal zones, it is desirable to examine the behavior of this quantity (conserved for adiabatic inviscid flow) during the

frontogenetical process. In our work, we will use the close approximation to Ertel's (1942) original expression given by

$$\text{IPV} \equiv -\eta_\theta \frac{\partial \theta}{\partial p} \tag{1}$$

where η_θ is the absolute vorticity, $\zeta_\theta + f$, measured on an isentropic surface.

The evident lack of condensation and evaporation in this type of frontogenesis makes IPV an attractive diagnostic quantity, and Reed (1955) found that it was indeed nearly conserved in a particular case. In contrast, Staley (1960) attributed a lack of conservation near the tropopause in an upper-frontal situation to a vertical gradient of diabatic heating due to turbulent heat flux. More recently, Shapiro (1976) suggested that this flux was responsible for creation of an anomalously high value of IPV in a mesoscale region of extraordinarily large cyclonic wind shear at the level of the jet core.

In our work, analyses of wind direction and speed on the 311-K and 295-K surfaces were the bases for natural-coordinate measurements of relative vorticity,

$$\zeta = -\frac{\delta V}{\delta n} - V\frac{\delta \psi}{\delta s}, \tag{2}$$

at the intersection of each 5° of latitude and longitude. Here V is the observed wind speed, ψ is the geographical wind direction and the n and s axes are to the left of and along the direction of flow, respectively. The mesh lengths, δn and δs, were 555 km. The stratification, $-\partial\theta/\partial p$, was approximated by the difference in pressure, obtained by graphical subtraction, over an interval of 8 K in virtual potential temperature, centered on either 311 or 295 K. The field of IPV was obtained by graphical multiplication, checked and slightly modified in places by reference to values at sounding stations.

Results are shown in Fig. 7, for the two levels and four times. At the 311-K surface, the isopleths for 1 and 2 "IPV units," followed the ribbon of maximum winds in the jet stream over much of the area of analysis. Hoskins et al. (1985) characterized 1.5 IPV units in their terms (which differ from ours by the factor g) as the tropopause.

On the 311-K surface there was no egregious evidence of nonconservation of IPV. The poleward extension of low values increased substantially from 2800 to 2812 (Figs. 7a,b), seemingly more than advectively, but the initial analysis just off the west coast of North America was uncertain. This extension later retracted in northwesterly flow (Figs. 7c,d), consistent with advection. The extreme isopleths of 8 and 0.25 IPV units appeared and disappeared from map to map, but the areas encompassed were small, and station values in their vicinities were close to these critical values throughout the period.

The evolution of the IPV field at 295 K, in contrast, shows a striking development. A trough of high values moved eastward with the deepening trough in the flow from 2800 to 2812 (Figs. 7a,b). The maximum value in this trough, about 1 IPV unit, moved southeastward consistent with advection. When the frontal zone developed in the middle troposphere at 2900 (Fig. 2c) however, the maximum value in this trough abruptly doubled (Fig. 7c). Maximum values near 2 IPV units continued as the system then moved into the southeastern states, again consistent with advection (Fig. 7d).

This growth of IPV will be shown to represent a large increase of the stratification without a proportionate reduction of isentropic vorticity, as would be required by conservation. Other large changes on the 295-K surface, due to diurnal changes in boundary-layer stratification, were seen near the intersection of this surface with the surface of the earth.

Some quantitative information on conservation, mainly in the northwesterly flow, can be obtained by comparing the values of IPV at the beginning and end of the 12-h isentropic trajectories discussed in section 3. These are shown for the interval from 2812 to 2900 in Fig. 8.

On the 311-K surface, most trajectories showed approximate conservation. The cluster in the lower left corner represents trajectories remaining in the tropospheric region of low IPV. With the higher values, there are a few striking examples of apparent nonconservation. For the most part an adjustment of less than 300 km in one of the end points of the trajectory would by itself have yielded conservation, aside from uncertainties in analysis of the IPV field itself.

These adjustments were not random vectors. Most of them required the point of origin to be farther SW, suggesting that our technique indicated too much clockwise turning occurring too early. Between 2800 and 2812 the isopleths of 1, 2 and 4 units advanced toward the northeast more rapidly than the normal component of geostrophic flow, suggesting that the actual flow just downstream from the upper ridge may have been more ageostrophic, and more toward lower geopotential than our analysis indicates.

Alternatively, the result may not be entirely due to error. Since the region where this apparent loss of IPV occurred was adjacent upstream from the region of evident gain on the lower surface, we may be seeing compensating dilution and concentration of IPV in the layers containing the two surfaces, as should occur (Haynes and McIntyre 1987). The limited number of observations, especially of wind, in Canada precludes a confident interpretation of the situation on the 311-K surface.

On the 295-K surface, the scatter diagram in Fig. 8b shows a different picture. Because of the smaller range of IPV values, the changes along the trajectories were smaller on the whole. (The selected trajectories avoided the region of large diurnal changes due to boundary-

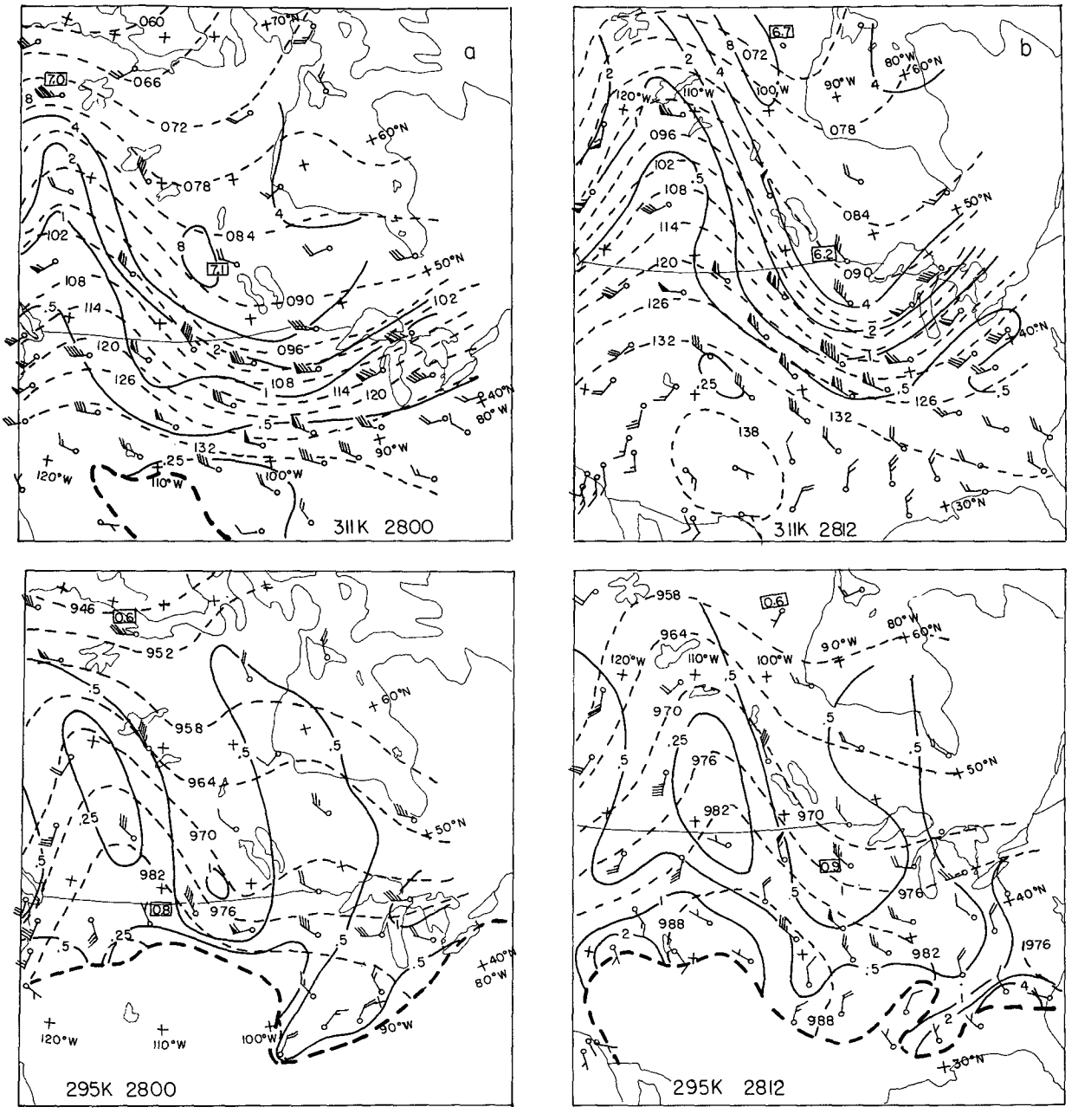

FIG. 7. Analyses for the 311-K and 295-K (virtual) isentropic surfaces, (a) for 2800, (b) for 2812, (c) for 2900, and (d) for 2912. Dashed lines are isopleths of Montgomery potential, $gz + c_p\theta(p/1000)^\kappa$, at intervals of 6×10^2 m^2 s^{-1}. Selected isopleths of IPV in units of 10^{-5} mb^{-1} s^{-1} are shown as solid lines, for consecutive values differing by a factor of 2. The heavy dashed line shows the surface position of the 307-K or 291-K virtual isentrope. Extreme values of IPV at selected sounding stations are shown as boxed numbers. Winds are plotted as in Fig. 2.

layer heating and cooling.) The two outlying points at 295 K in Fig. 8b are for trajectories from 2812 to 2900 terminating at stations in the frontal zone that appeared so dramatically in Fig. 2c. No trajectory adjustment can account for these changes.

The situation is illustrated in Fig. 9. Soundings at these two terminating points are shown in Figs. 9b,d, along with values of η, Δp, and IPV at these locations. For the points of origin of the 12-h trajectories ending at each station, the corresponding numerical data obtained by interpolation from the analysis 12 h earlier are given in parenthesis in Figs. 9a,c. The soundings nearest the points of origin also appear in Figs. 9a,c, with the bearing and distance from the sounding station to the point of origin also given in parentheses. By comparison of the final data in Figs. 9b,d with the initial

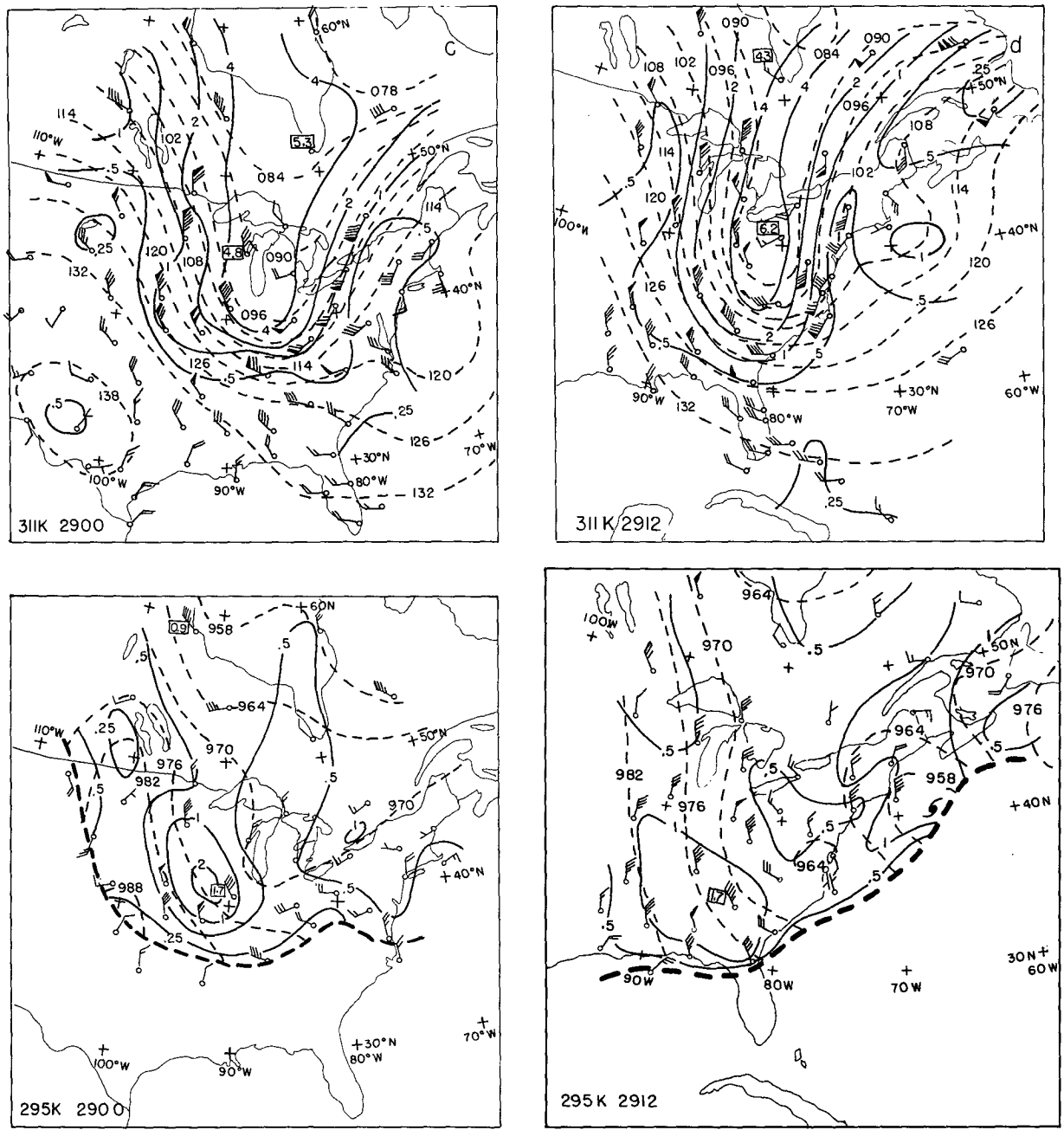

FIG. 7. (*Continued*)

data in parenthesis in Figs. 9a,c, it can be seen that in both cases the stratification and the IPV roughly doubled, with a slight decrease of absolute vorticity on the isentropic surface. The soundings nearest the points of origin confirmed the changes of stratification, although not of isentropic vorticity. Station 71867, nearest the point of origin for the trajectory terminating at station 72655, was rather far away from it, but none of the other soundings at 2812 showed the strong stability appearing later; and it would be difficult to gerrymander a region of large IPV values between stations at this time (Fig. 7b).

In the earlier interval from 2800 to 2812 (not shown), there were no large changes of IPV along trajectories on the 295-K surface. In the later interval (also not shown), a number of instances of either increase or decrease, of the magnitude shown in Fig. 8b, was seen. These could be explained, however, by modest errors in the trajectories or by involvement of the base of the layer used to measure stratification in boundary-

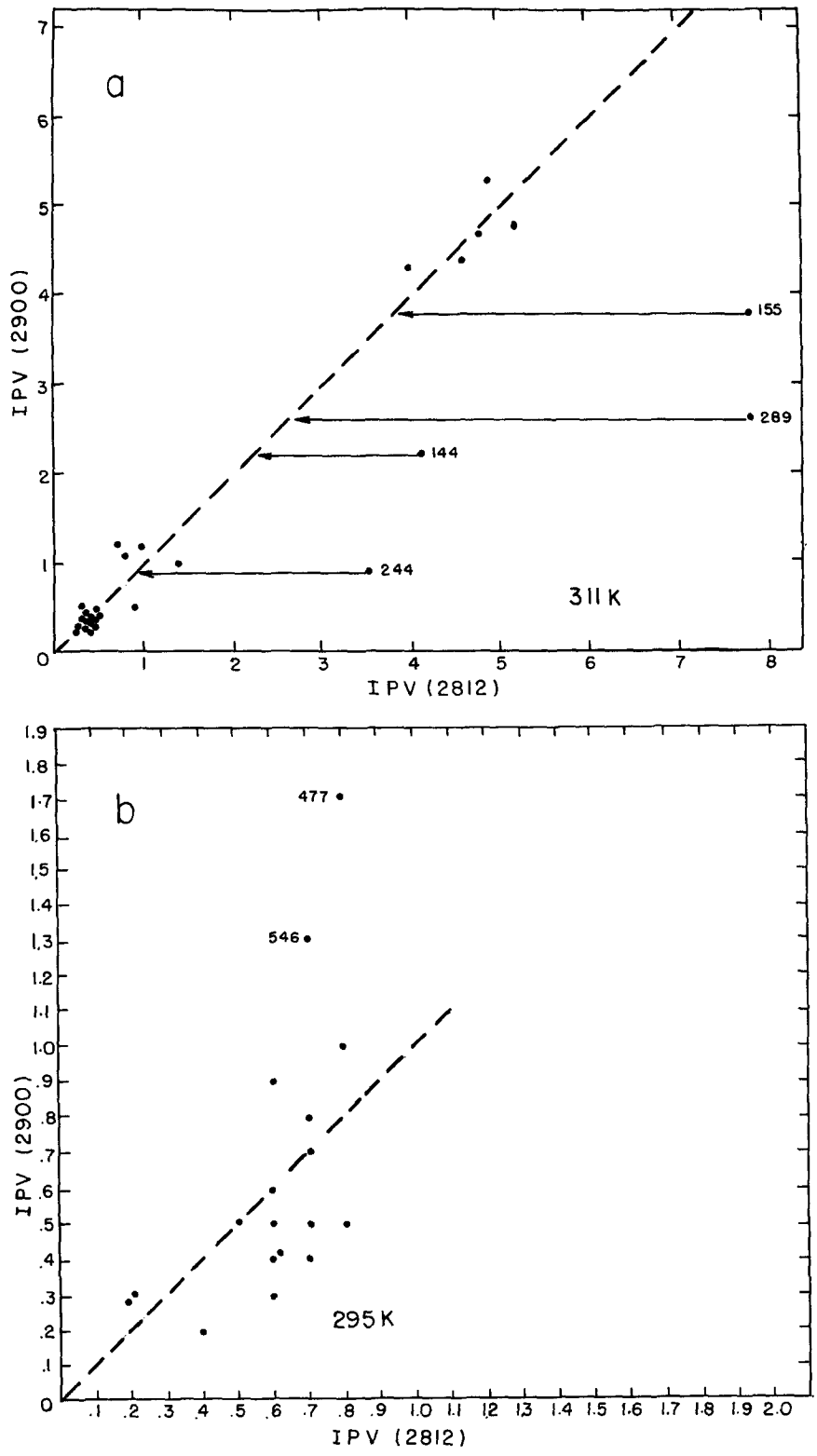

FIG. 8. Scatter diagrams of initial vs final value of IPV for 12-h trajectories used in Fig. 6 for the (a) 311-K and (b) 295-K isentropic surfaces. Ordinates and abscissas are labeled in IPV units of 10^{-5} K mb^{-1} s^{-1}. The numbers to the right of selected points in (a) are the distances in km required for initial position adjustments to yield values identical to the final station values. The numbers to the left of selected points in (b) are the final station values of pressure in millibars.

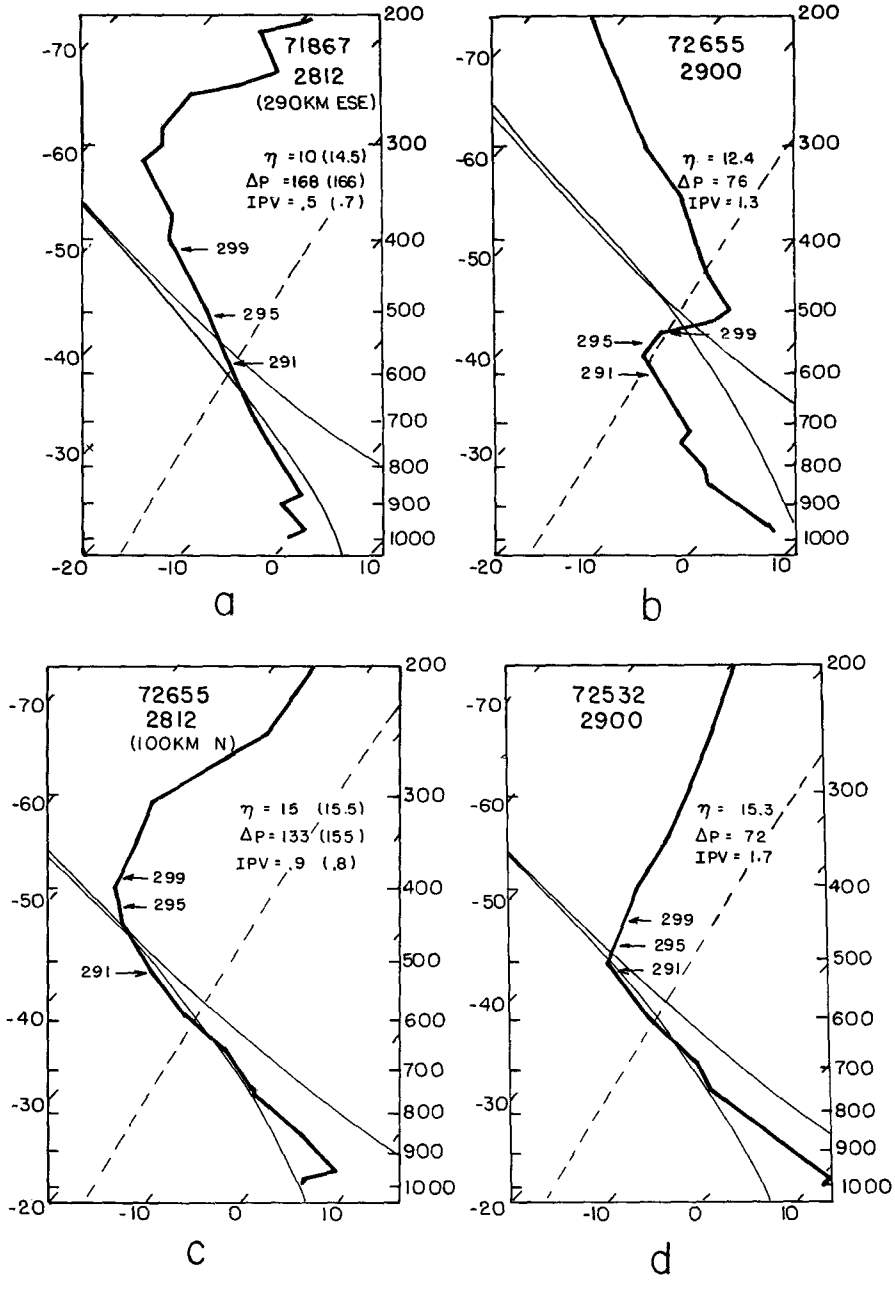

FIG. 9. Soundings of temperature on skew T–log$p$ diagrams illustrating large apparent changes of IPV on 12-h trajectories along the 295-K surface. Soundings are shown for stations (b) and (d) at the points of termination of the trajectories. Values of η, δp, and IPV are shown for these stations and also, in parenthesis in (a) and (c), respectively, for the points of origin of the trajectories. Soundings and data 12 h earlier for the stations nearest the points of origin are also shown in (a) and (c). The bearing and distance of the points of origin from the stations in (a) and (c) are shown in parentheses. Positions of selected virtual isentropic levels are shown by arrows. The heavy solid line represents temperature, and the thin solid lines indicate dry and saturation adiabats.

layer cooling. The only unambiguous growth of IPV occurred between 2812 and 2900, as the 295-K surface was absorbed into the developing frontal zone.

At 311 K, some apparently substantial decreases were noted in the earlier interval, not as large as between 2812 and 2900, on some trajectories in the region of northwesterly flow just downstream from the ridge. During the later interval comparably large changes were not seen. Although no interpretation of these observations can be offered with confidence, they are con-

sistent with the downward propagation of the frontal zone to lower elevations and potential temperatures shown in Table 1.

This downward migration might have been regarded as a result of inviscid adiabatic large-scale dynamics, had IPV been conserved. In this case, conservation would require the increasing stratification at the base of the zone to be accompanied by decreasing isentropic vorticity, but Figs. 7b,c showed that this did not happen. These figures also failed to show decreasing stratification and increasing absolute vorticity on isentropic surfaces near the top of the zone. The nonconservation of IPV points to turbulent transfers of heat and momentum as the responsible mechanism. The routine data are not sufficient to establish the relative importance of these ingredients. Thus we rely, however precariously, on the opinion of others (e.g., Staley 1960; Shapiro 1976) that the diabatic effect is likely to be dominant.

How this propagation of the frontal zone might work is illustrated schematically in Fig. 10. If turbulent heat transfer were the only mechanism of temperature change, we suggest that the change of the potential-temperature profile would produce the change from A to B. Maximum heating occurs near the base of the frontal zone and maximum cooling near the top, with some cooling continuing above but no heating below. This produces a migration of the boundaries of the zone toward colder potential temperature. The stratification increases just below the initial base of the frontal layer, but decreases within the layer itself, especially just below the initial upper boundary. Changes of IPV accompany the changes in stratification, with increases occurring just below the initial lower boundary and decreases elsewhere. Subsidence, however, begins at the base of the zone and increases upward toward the potentially warmer air, thus tending to restore the initial stratification, without further alteration of IPV, although the absolute vorticity on isentropic surfaces decreases. This decrease can be seen on the 295-K surface in Fig. 9, although we did not attempt to confirm the decrease of IPV above.

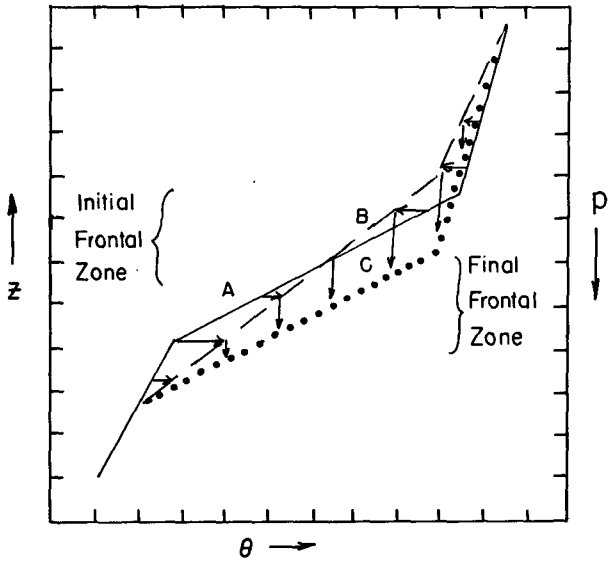

FIG. 10. Idealized vertical profile of potential temperature illustrating a hypothetical mechanism for migration of the frontal zone downward toward colder potential temperature. The initial profile is denoted by A. The modified profile resulting from turbulent heat transfer is the dashed line B, with horizontal arrows showing the diabatic heating or cooling. The dotted line C shows the final state, taking into account the frontal-scale subsidence, with arrows showing vertical displacement.

This picture would require intense downgradient heat fluxes within the frontal zone, with strong vertical gradients near the edges, where the warming and cooling are largest. These strong gradients might be expected because of reduced Richardson number in the frontal layer, since

$$\mathrm{Ri} \equiv \frac{g}{\theta}\frac{\partial\theta}{\partial z}\left(\left|\frac{\partial \mathbf{V}}{\partial z}\right|\right)^{-2}. \tag{3}$$

Reduced values in the zone would be anticipated within the zone if the isentropic slopes remain the same or become steeper in the frontogenetical process (c.f., Fig. 3c,d); because in this event the horizontal temperature gradient and thus the (balanced) vertical wind shear, the effect of which goes as the square in (3), would increase at least as rapidly as the stratification increases.

Browning and Watkins (1970) and Browning (1971) showed an example of reduced Ri in an upper-level frontal zone. In their case, values of Ri as small as 0.25 were found over very small vertical intervals. The effect of the resulting turbulence in their case was to produce infrastructure within the baroclinic zone. Bosart and Garcia (1974) also found numerous values of Ri < 1 in calculations based on 2-K intervals of potential temperature. Such detail was present in our case, to judge from the temperature soundings, but the limited vertical resolution of our wind data precluded a similar examination.

It was possible, however, to show reduced values of Ri over the depth of the frontal zone. For selected soundings in the northwesterly flow, or in the upstream ridge and downstream trough, Ri was calculated for each 4-K isentropic layer. The soundings were required to show maximum observed wind speeds of at least 33 m s^{-1} and a pronounced layer of strong vertical shear. From 2812 to 3000, 26 such soundings were selected. Averaged isentropic depths and wind shears for each time were used to calculate Ri from (3), with results plotted as inverse Ri in Fig. 11. The reduced values of Ri are evident, generally in the frontal zone of least isentropic depth (i.e., greatest stratification). Numerous instances of Ri $\leqslant 1$ can be seen.

Note that even in this limited sample of soundings the sinking of the frontal layer toward lower potential temperature was plainly evident. (Once the base of the

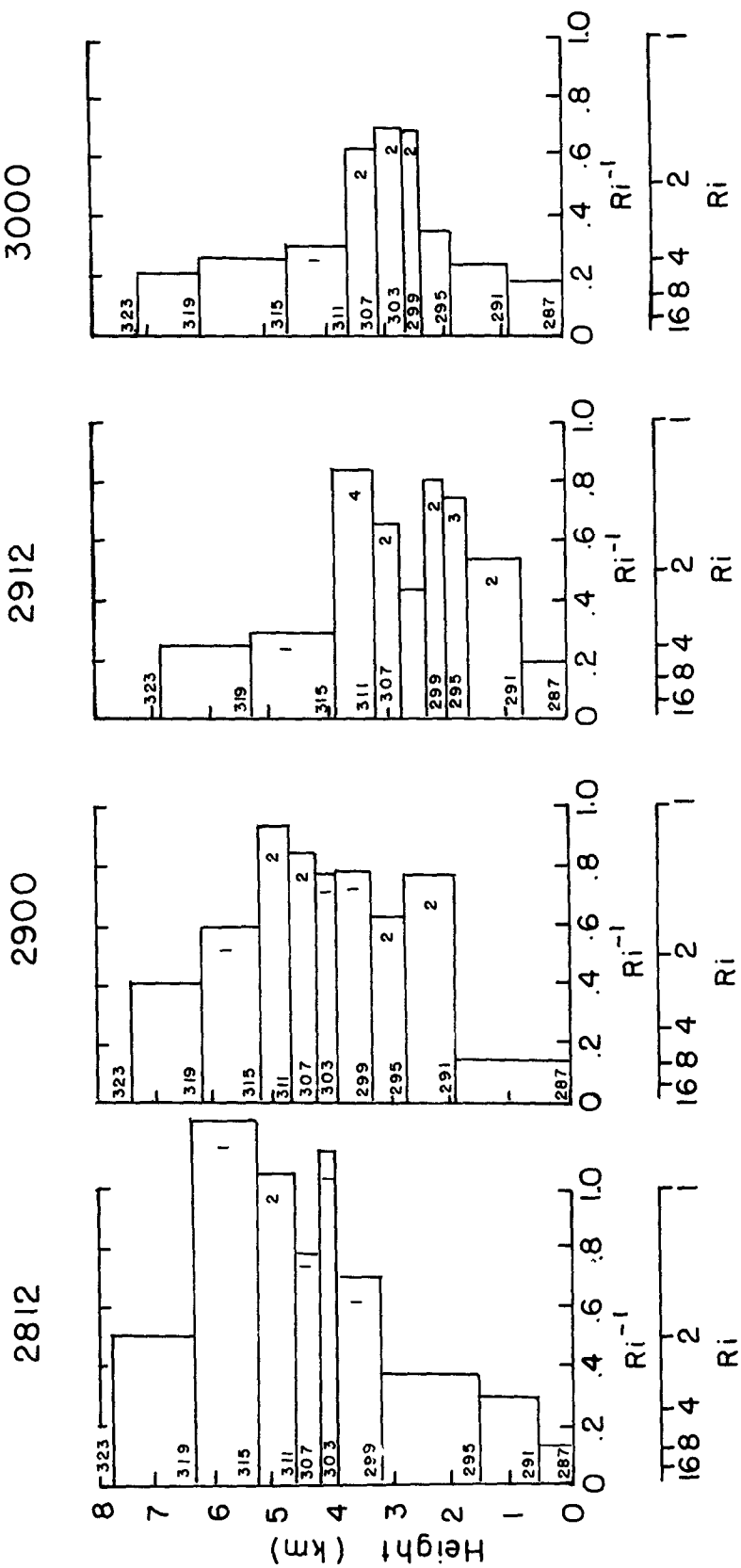

FIG. 11. For selected frontal soundings, mean Richardson number Ri vs elevation above height of 287-K isentropic surface, for 4-K isentropic layers: (a) for two soundings at 2812, (b) for six soundings at 2900, (c) for ten soundings at 2912 and (d) for eight soundings at 3000. Potential temperature (K) of interface between layers is shown. Numbers near right edge of layer boxes indicate numbers of individual soundings showing Ri $\leq$ 1 for the layer.

frontal layer reached the 291-K level it appeared to be in contact with a surface boundary layer that was well mixed during the daytime.)

The irregularities in Fig. 11 reflect complexities of structure in the individual soundings, within and outside the frontal layer. The limited extent of the data made further attempts to determine the details of IPV alteration impossible, but we conclude tentatively that turbulent heat flux produced the growth seen in Figs. 7b,c, and probably a loss in the upper part of the frontal zone.

5. Structure of the vertical wind shear

A sloping two-dimensional frontal zone characterized by stronger sinking motion in the warmer than in the colder air, as in this case, with little evidence of adjacent ascent in yet warmer air, implies locally a thermally indirect transverse circulation. With surface frontogenesis, on the other hand, the warm air rises relative to the cold air and the transverse circulation is thermally direct. An interpretation in this latter case is that the large-scale flow is producing an increase in horizontal temperature gradient while tending to weaken the vertical wind shear. The transverse circulation provides an increase of shear, tending to balance the growing temperature gradient while mitigating its growth through adiabatic warming and cooling.

For the upper-level front, an analogous interpretation would be that the vertical wind shear is too large for the horizontal temperature gradient. Although Keyser et al. (1989) have pointed to the danger of associating cross-contour flow aloft with vertical motion in a well-developed wave, the role of the indirect transverse circulation might then be to weaken the shear while enhancing the temperature gradient through adiabatic effects.

The most obvious possibility for strong vertical shear accompanying weak horizontal temperature gradients is gradient-wind balance in an upper-level ridge, with the supergeostrophic shear becoming excessive and requiring adjustment as the air subsequently flows toward the downstream trough. Newton and Palmen (1963), in fact, showed an example of vertical shear greatly in excess of the geostrophic (thermal-wind) value in a large-amplitude ridge in the upper troposphere, and attributed it to the effects of centrifugal force in the curving flow. Newton and Trevisan (1984) discussed the dynamical consequences of this kind of situation.

Consider gradient balance in an equivalent-barotropic warm ridge. The geostrophic flow increases upward and the curvature of the streamlines is uniform in the vertical. Because the excess of the gradient wind over the geostrophic increases as the latter increases, the vertical shear of the gradient wind exceeds the thermal wind.

If such a meridionally oriented ridge is progressing, say, eastward, then an additional effect arises, because of the difference between the curvatures of streamlines and of trajectories. The latter determines the centrifugal force. According to Blaton's Formula for a system propagating without change of shape, the two curvatures on the ridge line are related by

$$R_t = R_s(1 - c/V) - 1, \tag{4}$$

where the subscripts, t and s, refer to trajectories and streamlines, c is the phase speed of the ridge, and V is the wind speed. With uniform c, the flow is straight when the wind speed is equal to the phase speed, as it might be at a midtropospheric level. At higher levels with stronger wind speed, however, R_t decreases, approaching R_s as an upper limit where V is much larger than c, as might be the case near the jet core.

An equation for the gradient wind speed is

$$fV_g - V^2/R_t = fV, \tag{5}$$

where f is the Coriolis parameter and the subscript g denotes the geostrophic value. Substitution of (4) in (5) then yields, for the normal gradient wind,

$$V = 0.5\{c - fR_s - [(fR_s - c)^2 + 4fR_sV_g]^{0.5}\}. \tag{6}$$

We apply (6) for some particular cases. The ridge shown in Fig. 1 moved across western and central Canada at 13 m s^{-1}. During its period of greatest intensity, R_s was about 500 km. The sharp character of the ridge is evident in Fig. 2.

With $f = 10^{-4}$ s^{-1}, so that $fR_s = -50$ m s^{-1}, the profile of V as a function of V_g (which can be regarded as a vertical coordinate in this context) is shown in Fig. 12, starting with $V = V_g = 13$ m s^{-1}. As V_g approaches a mere 20 m s^{-1}, the wind shears very rapidly to 31.5 m s^{-1}, the limit of possible normal gradient-wind balance for these conditions. The profile for a contrasting case of a slow-moving broader ridge is also shown in Fig. 12. This profile is qualitatively similar, but the shear departs little from the geostrophic value until V_g exceeds 30 m s^{-1}, finally becoming large as the wind approaches the balance limit of 101.5 m s^{-1}.

Note that in both these cases, the limiting value for normal gradient balance occurs with wind speeds less than twice the geostrophic value. The factor 2 arises in dealing with a static situation, as noted by Petterssen (1956). In fact, the limiting ratio, at which the radical vanishes in our model is given, via (7), by $V/V_g = 2fR_s/(fR_s - c)$. It approaches 2 when c becomes small relative to fR_s, as in our second profile above. The behavior of V and V_g at the limit of gradient balance is shown in Fig. 13. If midlatitude values for f are considered, then it is clear that the limit departs significantly from 2 only for rather sharp, fast-moving ridges. We will pursue the significance of this situation subsequently.

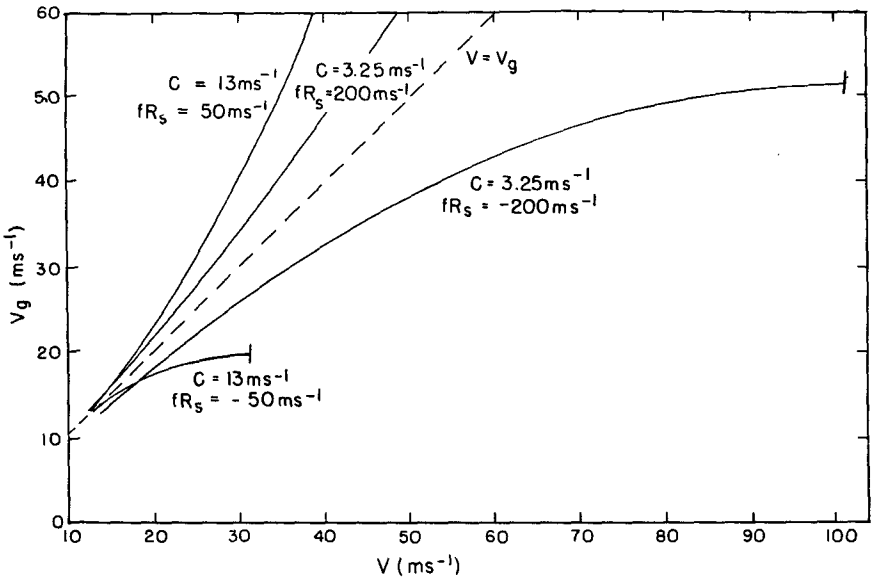

FIG. 12. For normal gradient-wind balance, profiles of V vs V_g for specified values of phase speed and of Coriolis parameter times radius of streamline curvature, positive cyclonic and negative anticyclonic. The dashed line is for purely geostrophic flow.

With cyclonic trajectories, the gradient wind speed at the base of our moving trough is given by

$$V = 0.5\{c - fR_s + [(fR_s - c)^2 + 4fR_sV_g]^{0.5}\}. \quad (7)$$

The profiles of V and V_g are shown in Fig. 12 for the trough in our case, in which the same magnitudes of c and fR_s are appropriate. Note that there is no sudden and dramatic increase of the wind shear relative to the geostrophic value, although large differences between gradient and geostrophic shears can occur.

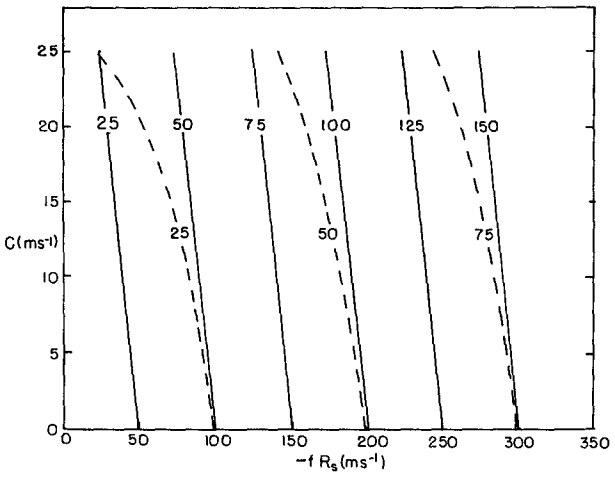

FIG. 13. Normal gradient-wind speed (solid lines, m s^{-1}) corresponding to specified values of maximum geostrophic speed for gradient balance (dashed line, m s^{-1}) for ranges of phase speed and of Coriolis parameter times radius of streamline curvature.

The rate of vertical shear at each isentropic level in our case was approximated by the vector difference over a centered interval of 8 K in potential temperature, divided by the corresponding pressure difference. This vector difference was normalized to represent a shear over 50 mb depth. All wind soundings displaying mid-tropospheric winds of at least 25 m s^{-1} were examined, from 2812 through 2912, from the ridge to about 500 km east of the trough. There were 54 such soundings. One of these was eliminated as erroneous.

For each isentropic level on each selected sounding the (geostrophic) thermal wind was estimated from the isentropic analyses. The thermal wind direction at each sounding station was obtained from orientation of the isentropic isobars. The magnitude was calculated by dividing the horizontal difference of pressure over 200 km normal to the isobars by the pressure difference over an interval of 8 K of potential temperature in the sounding. The magnitudes of the horizontal potential-temperature gradient and the geostrophic shear are related by

$$\left|\frac{\delta \mathbf{V}_g}{\delta p}\right| = \frac{R}{fp}\left(\frac{p}{1000\ \text{mb}}\right)^{\kappa}\left|\frac{\delta\theta}{\delta n}\right|.$$

The working formula is

$$\delta\theta = 0.007275p^{0.7146}(\sin\phi)|\delta \mathbf{V}_g|, \quad (8)$$

where $\delta\theta$ is a difference over 100 km in kelvin; $|\delta \mathbf{V}_g|$ is a difference over 50 mb, in meters per second; p is pressure in millibars; and ϕ is latitude. The ageostrophic shear was calculated by vector subtraction of the thermal wind from the shear of the observed wind. Results were quite noisy, especially just above the tropopause

where the 50-mb interval of the basic wind data was too large. Such layers with pressure thicknesses less than 25 mb were disregarded.

Among the remaining layers, 108 in which the magnitude of the ageostrophic shear exceeded 5 m s^{-1} per 50 mb (and was not obviously influenced by surface friction) were analyzed further. They were centered on the isentropic levels at each time as shown in Table 2. The temporal increase in the number of cases reflects in part the propagation of the strong shears from Canada to the United States. The drift toward lower potential temperatures is consistent with downward propagation of the frontal zone as discussed above.

The cases were stratified according to the position of the sounding station in the developing midtropospheric wave. Mean vectors, and their components along and normal to the thermal wind, for each position category are plotted with respect to the schematic wave in Fig. 14. The mean components and their large standard deviations are given in Table 3.

A systematic variation in the mean ageostrophic shear from the ridge to the downstream trough is seen in Fig. 14. The components along the thermal wind show supergeostrophic values in the ridge and subgeostrophic values in the trough, accompanied by geostrophic confluence, as in the "gradient wave" proposed by Newton and Trevisan (1984), and as found at 200 mb by Keyser et al. (1989) in their model calculation. The normal components are similar in the ridge to those found at 200 mb by Keyser et al. (1989), but elsewhere and overall show an oscillation similar to that implied in the "partial-inertial" wave of Newton and Tevisan (1984). They proposed such an oscillation, without geostrophic confluence, as a way of explaining wind maxima on ridges in the subtropical jet. It appears to be characteristic of at least this developing midlatitude wave as well.

In much of the northwesterly flow, in our case, the shear components toward higher temperature are qualitatively consistent with the subsidence in Fig. 6 and with ascent farther east. Here the circulation is thermally indirect despite the geostrophic confluence. The effect of the downstream change toward cyclonic curvature in this part of the wave evidently outweighs the effect of the confluence, which would otherwise be associated with a direct circulation. A similar effect was shown by Keyser et al. (1989). This part is the region in which strong frontogenesis is occurring on air parcels in the middle and upper troposphere as they flow into the developing frontal zone (Figs. 2 and 7).

The shear components to the left of the thermal wind in the ridge and just downstream are associated with flow in the upper troposphere across the contours toward lower height. This circumstance was noted by Bjerknes (1951), who interpreted it as a consequence of the inability of air parcels to follow the contours around the ridge in supercritical flow for which gradient-wind balance was impossible. Our earlier analysis (Fig. 12) supports that interpretation. He saw further that the consequence would be development of extremely strong winds in a jet streak around the downstream inflection point, subsequently crossing the contours at a small angle toward higher height, as also observed in Figs. 2 and 7 in this case. (At the jet-streak center itself the trajectory must be at least momentarily again parallel to the height contours, since the wind speed is at a maximum. At this moment the flow must be again in gradient balance, but the high speeds suggest that the balance represents the anomalous anticyclonic case. The partial-inertial oscillation then might be said to represent "trans-gradient" flow from the normal balance to the anomalous one, and then back to normalcy.)

Our interpretation diverges from Bjerknes's on the question of significance. His was that the process was of central importance for the growth of the baroclinic wave. We doubt that importance, since the growth of such a wave is explainable in quasi-geostrophic theory, in which large deviations from geostrophic balance do not occur, and since the effects occur in only a shallow portion of the vertical air column. We do propose, however, that this process is of central importance for the development of the upper-level front in this case.

A number of soundings that provide information on this partial-inertial oscillation and the initiation of the frontal zone are shown in Fig. 15. The two that provided the small sample of data in the ridge appear in Figs. 15a,b. The large shears at both locations were to the left of the thermal wind and much in excess of its speed (c.f., Fig. 14). Values of $Ri \leq 1$, calculated from (3), in these shear zones of modest moist stability were probably associated with strong turbulent heat fluxes. These would have acted in concert with the effect of the cross-thermal-wind component to produce the large stratification of the developing frontal zone.

The strong winds that defined the shear in these cases also resulted in the loss of wind data immediately above, leading one to wonder about the credibility of

TABLE 2. Count of center of qualifying isentropic layers 8 K deep in which the ageostrophic shear exceeded the rate of 5 m s^{-1} (50 mb)$^{-1}$.

Central potential temperature (K)	Date and UTC		
	2812	2900	2912
327	2	4	3
323	2	3	2
319	3	7	5
315	4	5	5
311	4	7	8
307	2	7	5
303	1	4	8
299	1	1	9
295	0	1	4
291	0	0	1

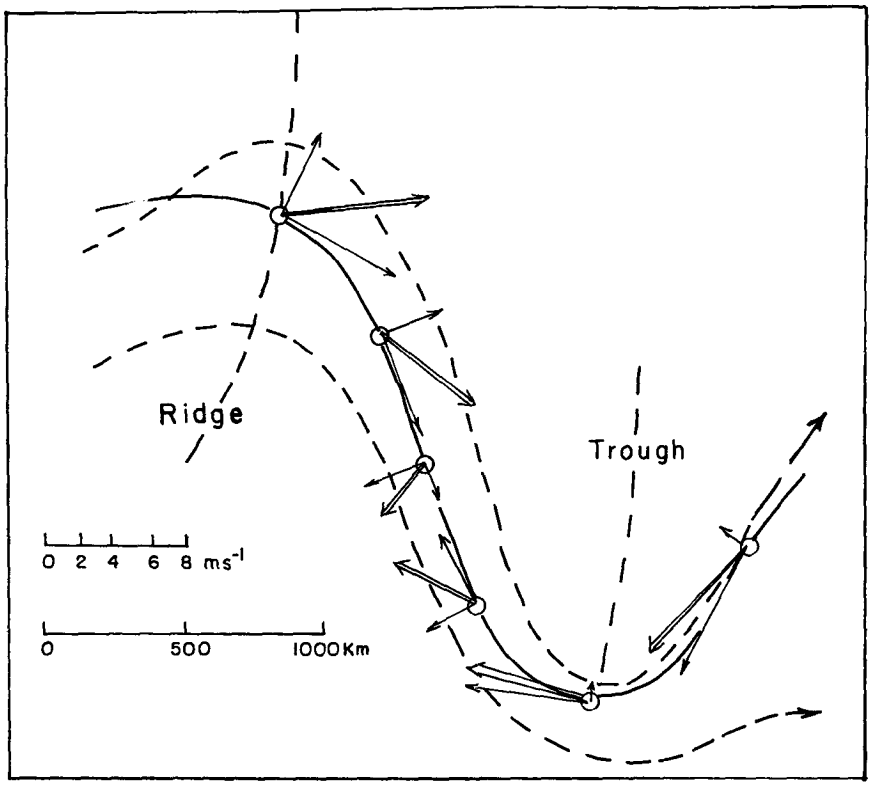

FIG. 14. Ageostrophic shear vectors (double-shafted arrows) and components (single-shafted arrows) for selected isentropic layers (see text), plotted relative to the temperature pattern in the schematic baroclinic wave with cold trough and warm ridge. The dashed lines represent contours of geopotential height or Montgomery potential. The solid line represents an isotherm, or an isentropic isobar, or a contour of difference in Montgomery potential across an isentropic layer.

the observations. Note, however, that these observations come from a time and place where we would expect the limit of gradient balance to have been exceeded. Note that the shear occurs as the wind speed exceeds the estimated limit of 31.5 m s^{-1} calculated for the hypothetical example in Fig. 12.

The two soundings with the largest ageostrophic shears near the inflection point are shown in Figs. 15e, f. Well-developed frontal zones appeared to be present between potential temperatures of about 303 and 311 K, but the strong wind shear continued into the layer of moderate stability above. The ageostrophic shears at 72747 were markedly to the right of the thermal wind through a deep layer, while at 72734 this was so only in the frontal layer itself. The shear was therefore weakening the stratification at both locations. Note from Fig. 2 that these two soundings were both poised at the upwind entrance region of the strongest horizontal wind.

The dry frontal layers in Fig. 15e,f cannot reasonably be identified with the moist ones at about the same potential temperature in Figs. 15a,b, even in consideration of the drying effects of strong subsidence. Careful estimates of the 12-h trajectories for the 319-K parcels terminating at 72747 and 72734 place their origins substantially farther north, respectively, nearest the soundings shown in Figs. 15c,d. At 71934 there was pronounced shear, to the left of the thermal wind, in the vicinity of the tropopause, where the wind speed closely approached the limit for gradient balance. At

TABLE 3. Components of ageostrophic shear (m s^{-1}) along (s) and normal (n, positive to the left) to the thermal wind, for selected isentropic layers (see text), stratified according to position within the baroclinic wave. Standard deviations are in parentheses.

Near ridge	500 km east of ridge	Inflection point	500 km west of trough	Near trough	500 km east of trough
N 5	5	26	9	57	6
+7.6 +4.2	+5.8 +2.6	+2.1 −3.1	−4.1 −3.3	−7.1 +0.8	−8.0 +2.0
(3.1) (2.4)	(1.6) (3.8)	(8.7) (6.3)	(7.3) (5.8)	(5.8) (4.7)	(4.4) (2.3)

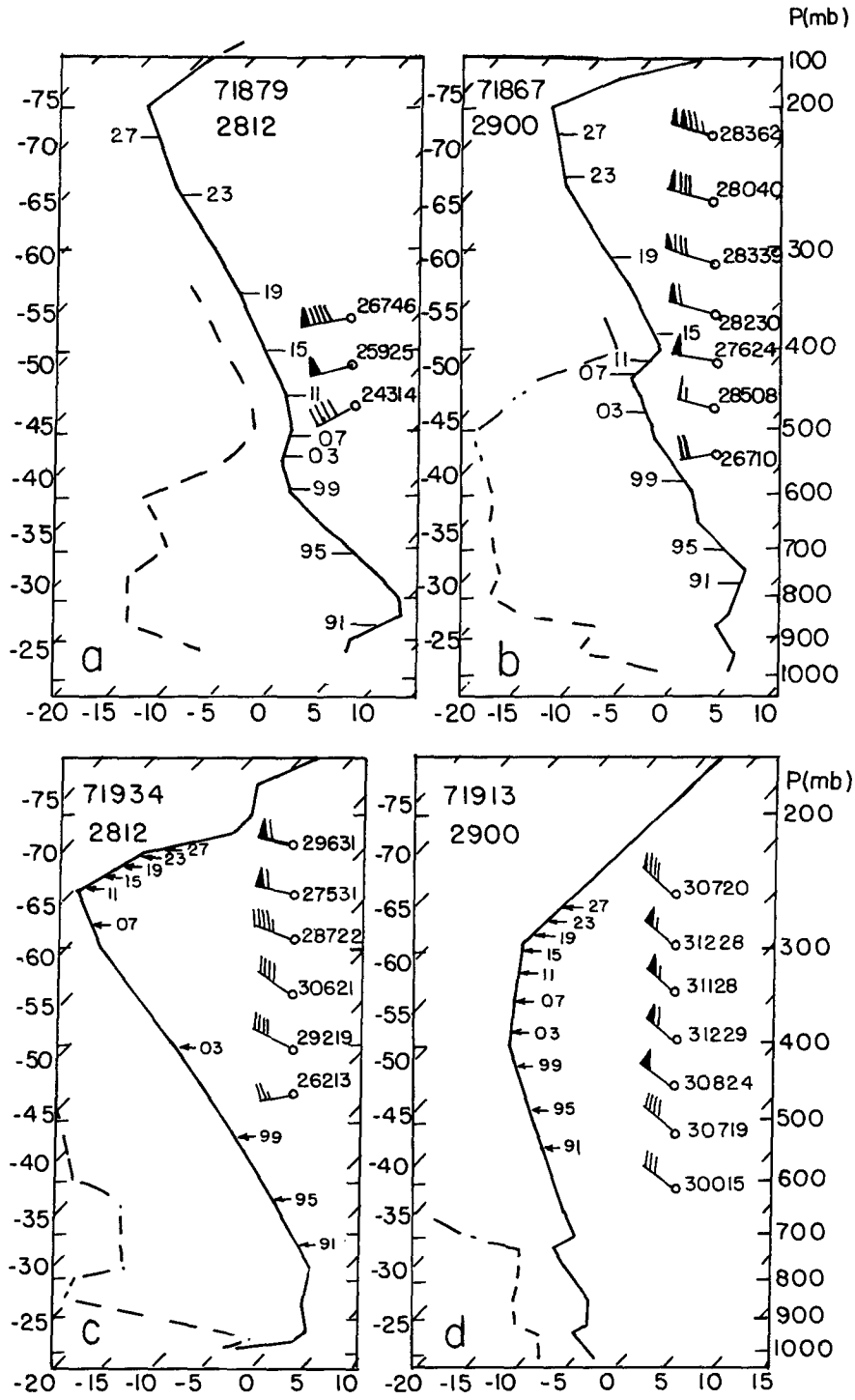

FIG. 15. Soundings for indicated stations and times, on skew T–log$p$ diagrams. Solid and dashed lines are profiles of temperature and dewpoint, respectively. Position of analyzed isentropic levels from 291 to 327 K are indicated. Wind directions and speeds (m s^{-1}) given at selected 1-km intervals. Strong ageostrophic shears are shown near the ridge, (a) and (b), and near the downstream inflection point, (e) and (f). Soundings (c) and (d) are from stations nearest the estimated points of origin of 12-h trajectories terminating in the layers of strongest wind at (e) and (f), respectively.

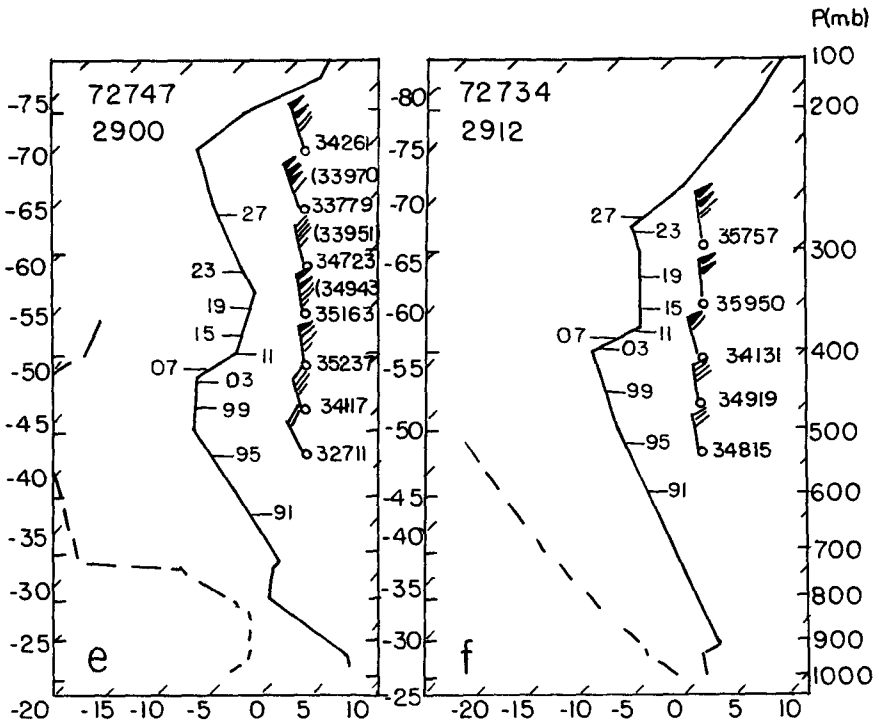

FIG. 15. (*Continued*)

71913 there was much weaker shear and no sharp tropopause.

Along both trajectories there was evidently much change in the stratification, inconsistent with the simple idea of a descending and folding tropopause. At the end points (Figs. 15e,f) there was large stability in the isentropic layer from 303 to 311 K, much larger than in the corresponding layer near the beginning points (Figs. 15c,d). On the other hand, in the layer from 319 to 327 K, the stratification probably decreased markedly along the 12-h trajectories. The sharp tropopause initially at 71934 (Fig. 15c) could not be seen 12 h later at 72747 (Fig. 15e). Nor could the weaker WMO tropopause initially at 295 mb at 71913 be found 12 h later at 72734.

Aside from the effects of the ageostrophic transverse circulation on the stratification, the restructuring was consistent with the effects of turbulent heat flux, provided there was a maximum downgradient flux in the layer from 311 to 319 K. Values of Ri near or less than 1 were found in this layer in both final soundings, consistent with this idea.

In both pairs of soundings there was a major increase of the maximum wind speed from the earlier to the later time (Figs. 15c–e and Figs. 15d–f), yet the winds at the termination of the 12-h trajectories were directed to the right of the thermal wind. Since at the top of the shear layer the motion to the left at the time and place of origin was apparently only starting, it appears that the partial-inertial oscillation had a half-period of less than 12 h.

This analysis of the vertical wind shear used only a selected fraction of the data, the bulk of which was quite noisy. To obtain a consensus for the bulk of the data, averaging over deep layers was necessary. To this end the entire layer from 291 to 315 K was considered, for the period from 2800 through 2912. It encompassed the fully developed frontal zone by the end of the period.

The mean pressure and depth of this layer is shown in the upper parts of Fig. 16. The mean pressure shows the layer to be midtropospheric except at its southern fringe. The depth was 400–500 mb in the major ridge and initially 250–300 mb in the cold trough. As the front developed, a small area with a reduced depth of less than 150 mb appeared in the cold trough, and then enlarged (Figs. 16c,d). This development corresponded to the growth of IPV in the colder portion of the frontal zone, as discussed above. Substantial fluctuations between evening (0000 UTC) and dawn (1200 UTC) were due to heating and cooling of the surface boundary layer.

The geostrophic flow and its vertical variation through the depth of the isentropic layer (the thermal wind) are shown, respectively, in the lower parts of Fig. 16 by the patterns of Montgomery potential M in the middle of the layer and the fields of its difference between the top and bottom of the layer. The ageo-

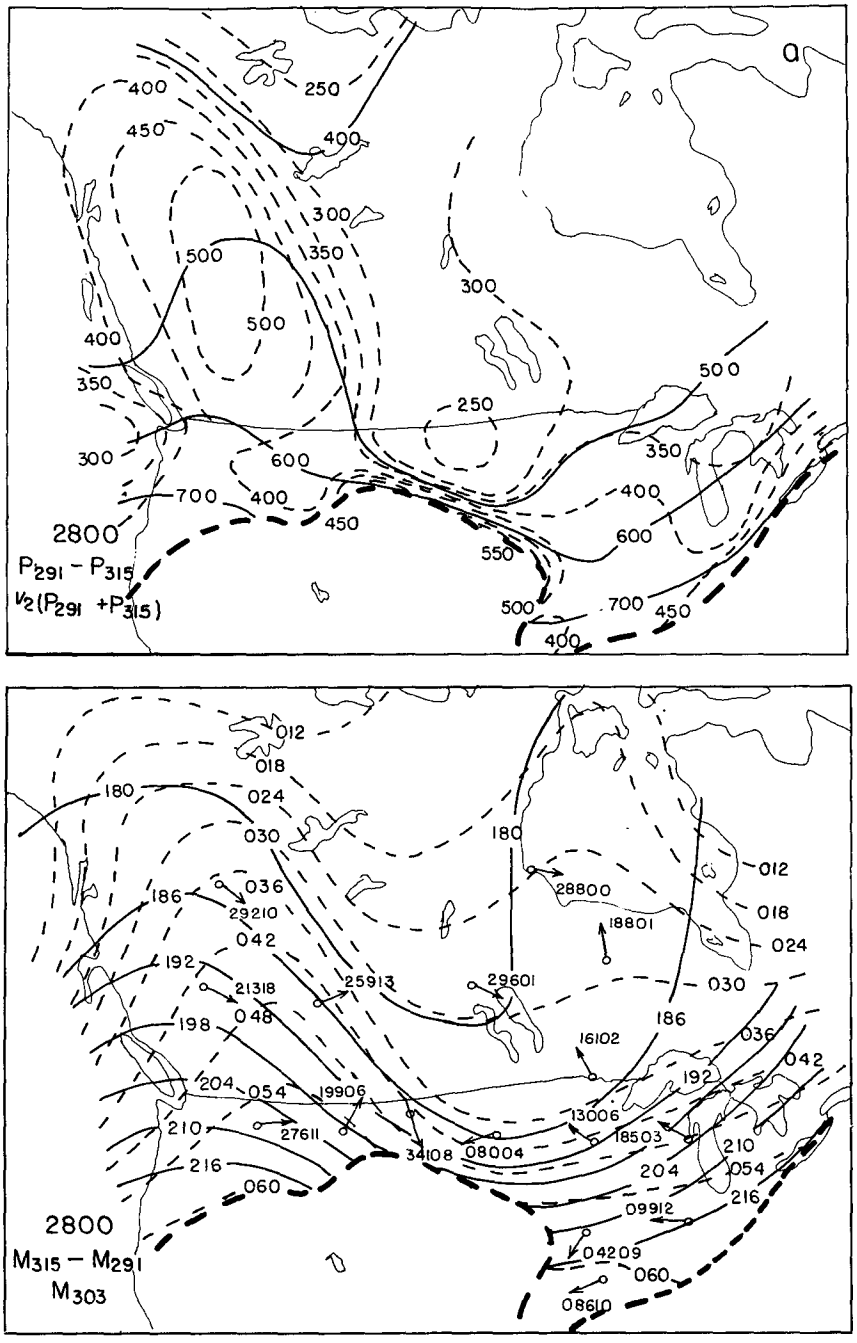

FIG. 16. Analysis of the isentropic layer from 291 to 315 K, (a) at 2800, (b) at 2812, (c) at 2900 and (d) at 2912. In the upper portions, solid lines are isobars of average pressure (mb) and dashed lines are isobars of the difference in pressure over the depth of the layer. The heavy dashed line is the intersection of the 291-K isentrope with the surface of the earth. In the lower portions, the dashed lines represent isopleths of Montgomery potential M, on the 303-K surface, at intervals of 6×10^2 m^2 s^{-2} on the 303-K surface. The solid lines are isopleths of the difference of M (δM) from the bottom to the top. The three-digit direction (degrees) and two-digit speed of the layer-averaged ageostrophic shear (m s^{-1}), calculated at each interior sounding station, is plotted numerically and as an arrow of arbitrary length. Labels for the M contours omit the leading "1."

strophic shears appear here as well. As the trough intensified and the upstream ridge became less sharp, the ageostrophic shears became more intense in the trough and weaker in the ridge. They were for the most part in the direction of the geostrophic flow in the ridge and opposed to it in the trough. The components east of

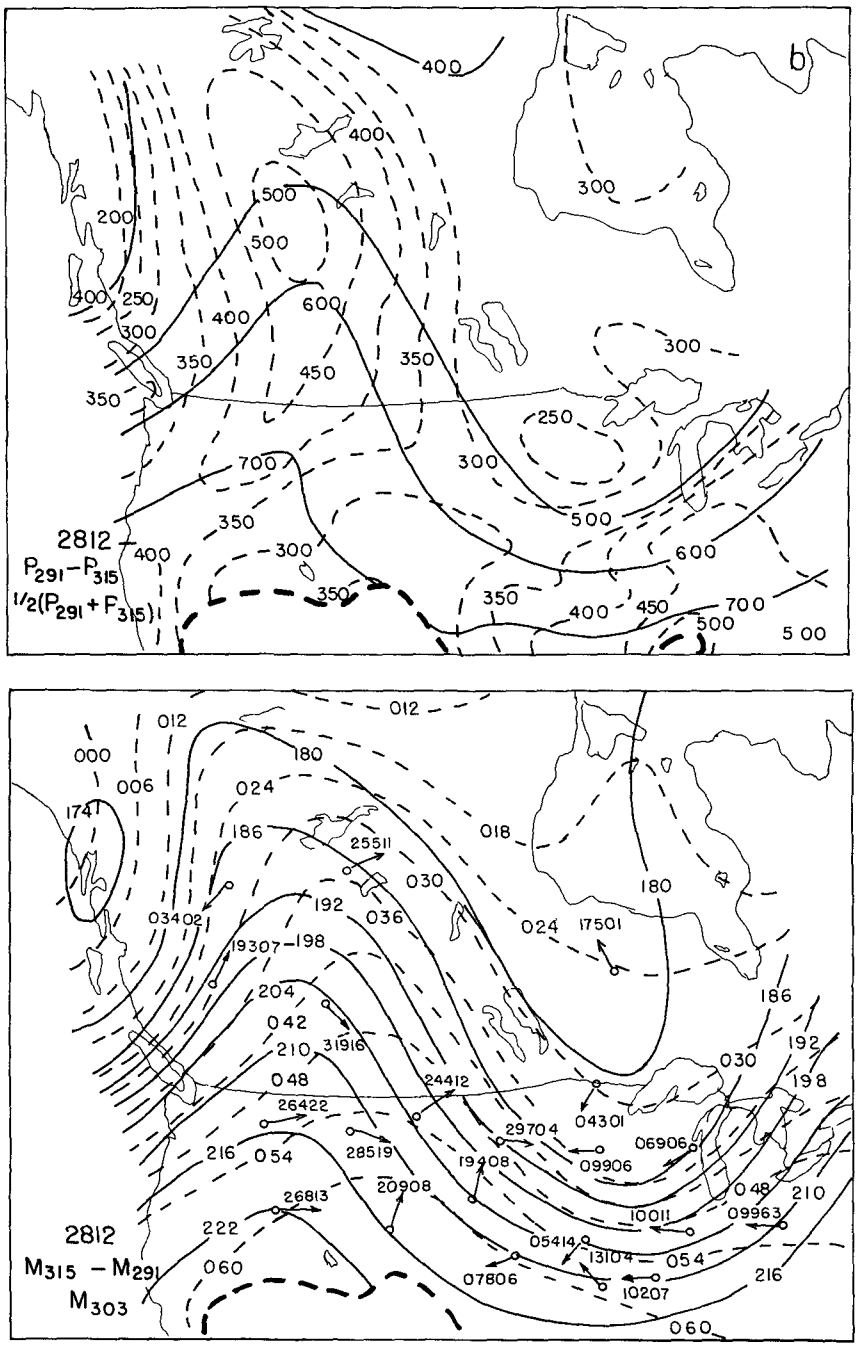

FIG. 16. (*Continued*)

the trough were mainly to the left of the thermal wind, as were those in and just east of the ridge. Components to the right appeared to be in the majority just west of the trough and around the inflection point.

On the whole, the results support the schematic (Fig. 14), although much variability persists, even after vertical averaging. Conditions in the ridge were not well documented, owing to limited wind observations in Canada.

6. Concluding discussion

We now return to address some of the questions raised by Keyser and Shapiro (1986), having documented the origin of an intense upper-tropospheric front and its growth to maturity. Its demise over the Atlantic could not be studied.

1) The mechanism of upper-level frontogenesis resembled in some respects that which was found in two-

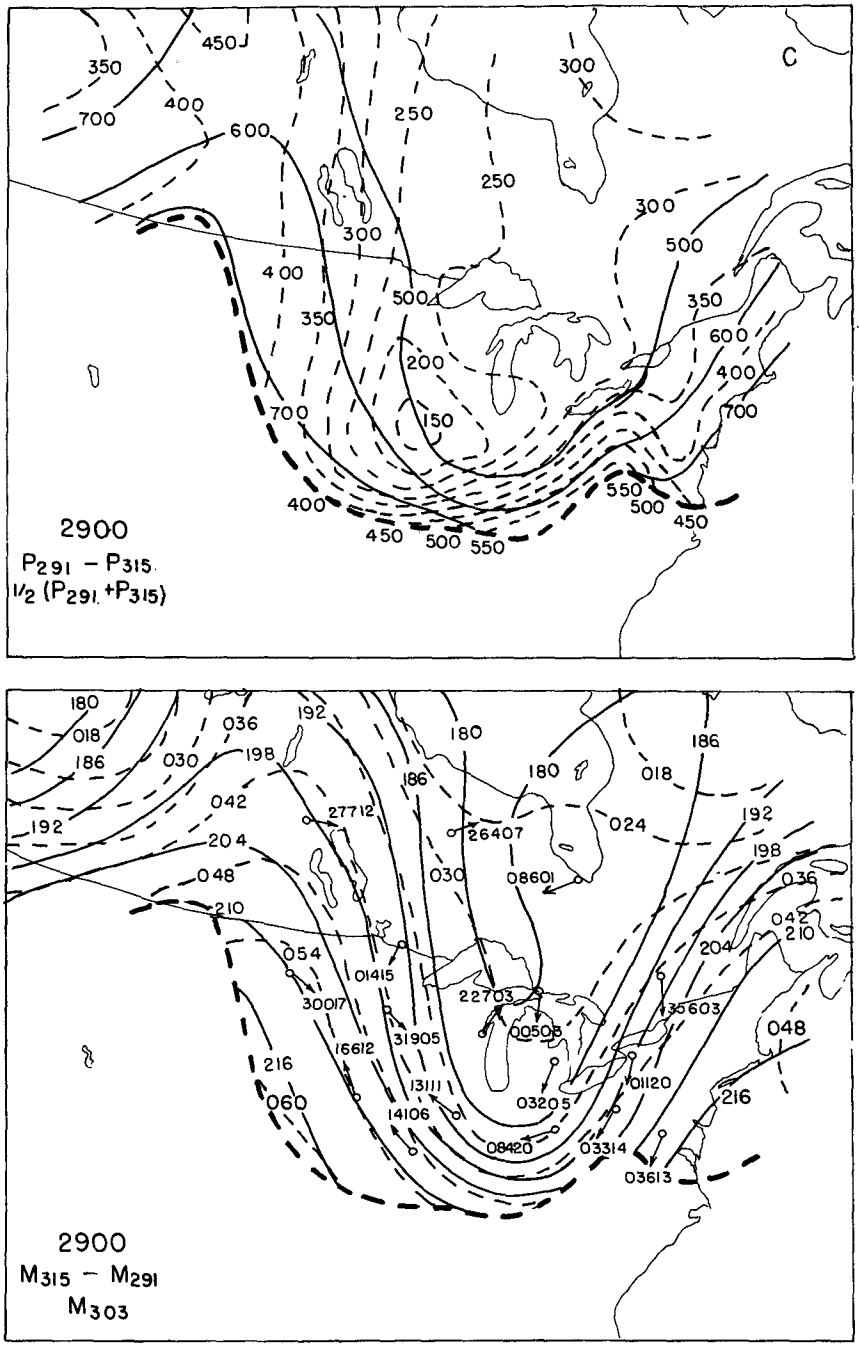

FIG. 16. (*Continued*)

dimensional modeling. The major region of subsidence (Fig. 6) between the upper ridge and the downstream upper trough was elongated in the direction of northwesterly flow, indicating that the cross-stream component of ageostrophic wind played a more important role than did the along-stream component. Keyser et al. (1989) have proposed that this comparison be used to assess two-dimensionality. Further, there was confluence in this upper flow (Figs. 2 and 7), as in two-dimensional models.

In other respects, however, the third dimension appeared to be important. The cold advection required in two-dimensional modeling (Keyser and Pecnick 1985) to produce realistic upper-level frontogenesis, was not present in precisely that portion of the northwesterly flow where Lagrangian frontogenesis first oc-

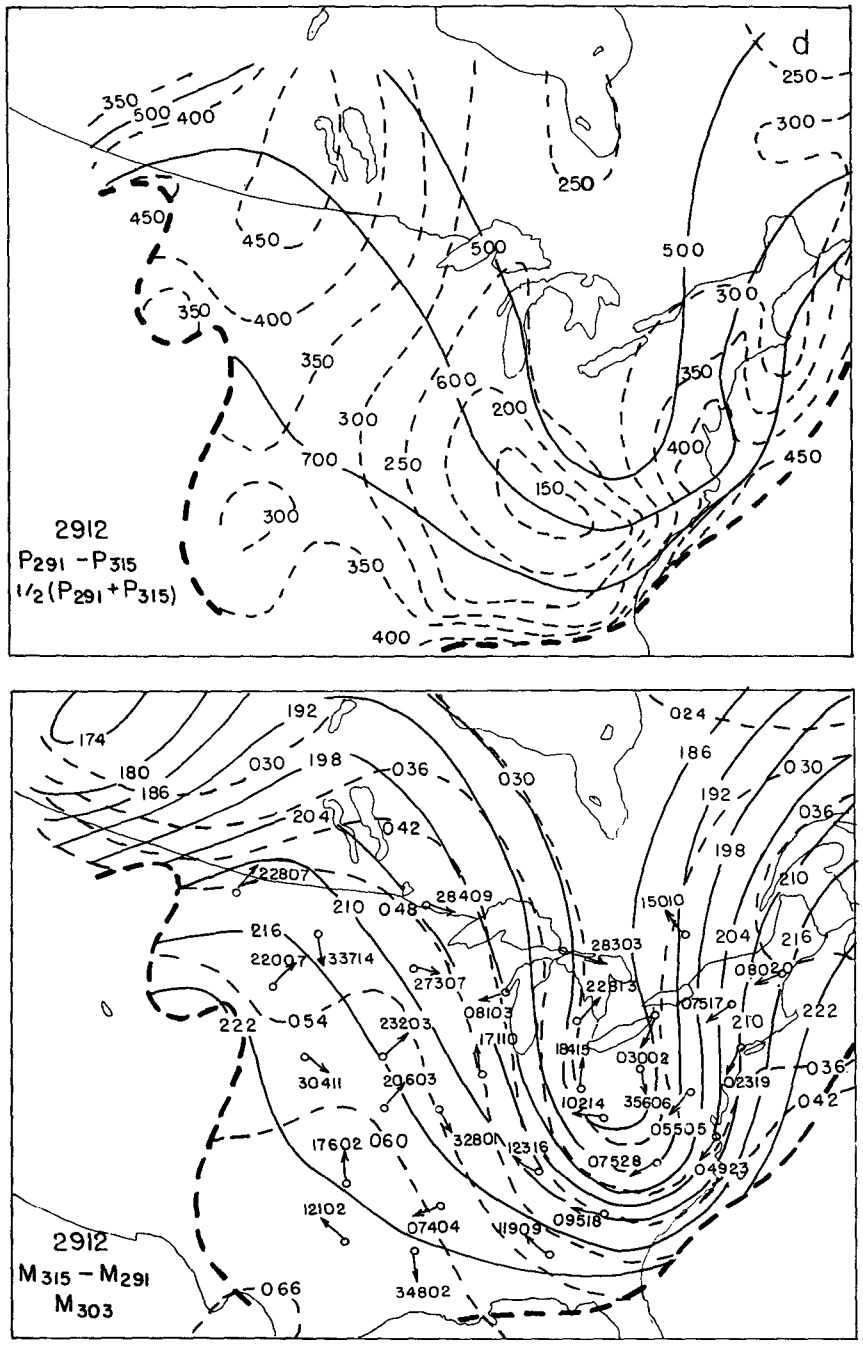

FIG. 16. (*Continued*)

curred (Figs. 2 and 6), although it was generally characteristic of the region between the upper ridge and the downstream trough. Examination of Figs. 2 and 3 also shows growth of the frontal zone with time, both vertically and along the flow, from a quite localized beginning. Even though the cross-stream variation of subsidence was dominant where the front first formed, the frontogenesis was evidently occurring along only a limited segment of the flow. The wave structure determined the location of this segment.

2) From the ridge to just beyond the downstream inflection point in the upper wave there was evidence of a "partial-inertial" oscillation somewhat resembling the type discussed by Newton and Trevisan (1984) in the subtropical jet. In the present case, however, the oscillation developed in a sharp mobile ridge in which

the geostrophic wind above the middle troposphere was stronger than the maximum value for which gradient balance is possible. The air accelerated while traveling on an anticyclonic trajectory with a component down the pressure gradient, then turning within 12 h to reach the inflection point with a component against the pressure-gradient force, despite confluence there. This same paradox was noted by Shapiro and Kennedy (1981) in aircraft measurements and by Keyser et al. (1989) in their model calculations.

The upper flow toward higher height was part of the thermally indirect circulation characteristic of the development of upper-level fronts, and the entire oscillation appeared to be of central importance for the initial development of the frontal zone in this case. The importance of this oscillation was an unexpected result. We cannot claim that it is always a necessary ingredient for upper-level frontogenesis. Although such a development downstream from a sharp mobile upper ridge is often observed, a counterexample is provided by Reed and Sanders (1953) in their first analysis of a case of this type of frontogenesis. In their case, the development appeared to be within relatively straight west-northwesterly flow, far from any prominent ridge, except in the Rocky Mountains beneath.

3) In this case the frontogenesis appeared to be a consequence of the intensification of the baroclinic wave, rather than a necessary precondition, since intensification was under way before the appearance of great frontal intensity. There was little frontogenetical response to the early stage of intensification.

4) There was at first little evidence of accompanying low-level frontogenesis, or of coupling with a low-level development, as envisioned by Uccellini and Johnson (1979). The northward motion and deepening of Hurricane Ginny on the 29th were far removed horizontally from the major action aloft.

Later, however, there was important surface frontogenesis and cyclogenesis in the wake of Ginny and immediately in advance of the cold upper trough. The upper front had reached peak intensity at this time. This cyclogenesis was typical of the western Atlantic on the approach of an upper-level trough. We did not attempt to assess the significance of the strong frontal zone embedded within the upper trough, especially as the low-level development occurred over the ocean. The upper and lower fronts did not merge.

Another unexpected result, not related to questions raised by Keyser and Shapiro, was the migration of the frontal zone to a lower range of potential temperatures as development proceeded. This process was accompanied by nonconservation of isentropic potential vorticity and calls into question the simple concept of lowering and folding of the preexisting tropopause during upper-level frontogenesis. Turbulent heat flux associated with reduced Richardson numbers within the frontal zone appeared to be the responsible mechanism for this migration and nonconservation. (In fact, the greatest value in analysis of IPV may ultimately turn out to be in its use of otherwise extremely difficult diagnosis of diabatic and frictional effects.)

Finally, the question arises whether this case of frontogenesis was truly extraordinary. A cursory examination of North American analyses over the past few cold seasons indicates that abrupt ridge building followed by frontogenesis of about this magnitude is not uncommon. It is strongly regime-dependent but averages about one case per month. Most often, however, there are a number of mobile features, superposed on a quasi-stationary planetary-scale wave of considerable amplitude, with the ridge in the eastern Pacific or the West Coast.

What is unusual in the case studied is its simplicity and the nearly zonal flow out of which it evolved. What made it unusually advantageous is that the building ridge and the initiation of frontogenesis occurred within the reach of the rawinsonde network over the continent. The primary limitation was the lack of jet-level wind observations over Canada, which might be remedied by analysis of a more recent case.

Needless to say, it would be of extreme interest to see whether a mesoscale numerical model can simulate all the features disclosed by our analysis. If not, then those features not simulated would remain unknown if only mesoscale model output, for all its advantages, were studied.

Acknowledgments. The authors are grateful to Dan Keyser, of the State University of New York at Albany, for the initial challenge motivating this study, for pointing out neglected aspects of our investigation, and for arguing spiritedly (if not always successfully) with us concerning our interpretations. Thanks are due to Isabelle Kole for drafting the many figures. The research was supported by the National Science Foundation under Grants ATM-8804110, 880550, and 880341, and by the Office of Naval Research under Contract N00014-87-K-0209.

REFERENCES

Berggren, R., 1952: The distribution of temperature and wind connected with active tropical air in the higher troposphere and some remarks concerning clear air turbulence at high altitude. *Tellus,* **4,** 43–53.

Bjerknes, J., 1951: Extratropical cyclones. *Compendium of Meteor.* T. F. Malone, Ed., Amer. Meteor. Soc., 577–598.

Bosart, L. F., 1970: Midtropospheric frontogenesis. *Quart. J. Roy. Meteor. Soc.,* **96,** 442–471.

——, and O. Garcia, 1974: Gradient Richardson number profiles and changes within an intense mid-tropospheric baroclinic zone. *Quart. J. Roy. Meteor. Soc.,* **100,** 593–607.

Browning, K. A., 1971: Radar measurements of air motion near fronts. *Weather,* **26,** 230–240.

——, and C. D. Watkins, 1970: Observations of clear air turbulence by high power radar. *Nature,* **227,** 260–263.

Ertel, H., 1942: Ein neuer hydrodynamischer Wirbelsatz. *Meteorol. Z.,* **59,** 271–281.

Haynes, P. H., and M. E. McIntyre, 1987: On the evolution of vorticity

and potential vorticity in the presence of diabatic heating and frictional or other forces. *J. Atmos. Sci.*, **44**, 828–841.

Hoskins, B. J., M. E. McIntyre and A. W. Robertson, 1985: On the use and significance of isentropic potential vorticity maps. *Quart. J. Roy. Meteor. Soc.*, **111**, 877–946.

Keyser, D., and M. J. Pecnick, 1985: A two-dimensional primitive equation model of frontogenesis forced by confluence and horizontal shear. *J. Atmos. Sci.*, **42**, 1259–1282.

——, and M. A. Shapiro, 1986: A review of the structure and dynamics of upper-level frontal zones. *Mon. Wea. Rev.*, **114**, 452–499.

——, B. D. Schmidt and D. G. Duffy, 1989: A technique for representing three-dimensional vertical circulations in baroclinic disturbances. *Mon. Wea. Rev.*, **117**, 2463–2494.

Newton, C. W., and E. Palmen, 1963: Kinematic and thermal properties of a large-amplitude wave in the westerlies. *Tellus*, **15**, 99–119.

——, and A. Trevisan, 1984: Clinogenesis and frontogenesis in jetstream waves. Part I: Analytic relations to wave structure. *J. Atmos. Sci.*, **41**, 2717–2734.

Petersen, R. A., and L. W. Uccellini, 1979: The computation of isentropic atmospheric trajectories using a "discrete model" formulation. *Mon. Wea. Rev.*, **107**, 566–574.

Petterssen, S., 1956: Motion and motion systems. *Weather Analysis and Forecasting*, Vol. 1., 2d ed. McGraw-Hill, 62–63.

Reed, R. J., 1955: A study of a characteristic type of upper-level frontogenesis. *J. Meteor.*, **12**, 226–237.

——, and F. Sanders, 1953: An investigation of the development of a midtropospheric frontal zone and its associated vorticity field. *J. Meteor.*, **10**, 338–349.

Sanders, F., 1954: An investigation of atmospheric frontal zones. ScD thesis, Massachusetts Institute of Technology, 132 pp. [Copy can be obtained from the author.]

——, 1986: Explosive cyclogenesis over the west-central North Atlantic Ocean, 1981–1984. Part I: Composite structure and mean behavior. *Mon. Wea. Rev.*, **114**, 1781–1794.

Shapiro, M. A., 1976: The role of turbulent heat flux in the generation of potential vorticity in the vicinity of upper-level jet stream systems. *Mon. Wea. Rev.*, **104**, 892–906.

——, and P. J. Kennedy, 1981: Research aircraft measurements of jet stream geostrophic and ageostrophic flows. *J. Atmos. Sci.*, **38**, 2642–2652.

Staley, D. O., 1960: Evaluation of potential-vorticity changes near the tropopause and the related vertical motions, vertical advection of vorticity, and transfer of radioactive debris from stratosphere to troposphere. *J. Meteor.*, **17**, 591–620.

Uccellini, L. W., and D. R. Johnson, 1979: The coupling of upper and lower tropospheric jet streaks and implications for the development of severe convective storms. *Mon. Wea. Rev.*, **107**, 682–703.

——, P. J. Kocin, R. A. Petersen, C. W. Wash and K. F. Brill, 1984: The Presidents' Day Cyclone of 18–19 February 1979: Synoptic overview and analysis of the subtropical jet streak influencing the pre-cyclogenetic period. *Mon. Wea. Rev.*, **112**, 31–55.